Chapter 2
Temperature Coefficients of Photovoltaic Devices

Abstract This chapter introduces the concept of temperature coefficient which enables to quantify the temperature sensitivity of the performances of photovoltaic devices. The temperature sensitivity of a photovoltaic converter originates from the temperature dependence of the fundamental conversion losses and of the bandgap of the absorber. The detailed balance principle is used to derive the fundamental losses which set the maximum of photovoltaic conversion efficiency in the radiative limit. It is highlighted that the unusual temperature dependence of the bandgap of perovskite compounds will ultimately result in peculiar temperature sensitivities. Following the discussion on the fundamental losses, the additional losses limiting the efficiency of present commercial cells are considered. The different loss mechanisms that drive the temperature coefficients of important cell parameters (open-circuit voltage V_{oc}, short-circuit current density J_{sc}, fill factor FF) are identified. The analysis shows how each of these temperature coefficients can provide some insight into device physics. The temperature sensitivity of open-circuit voltage is connected to the balance between generation and recombination of carriers and its variation with temperature. The temperature sensitivity of short-circuit current is driven by the bandgap temperature dependence and the incident spectrum on one hand and on the temperature dependence of the collection efficiency of the device on the other hand. As for the fill factor temperature sensitivity, it is ideally closely related to the open-circuit voltage temperature sensitivity but it also depends for certain devices on technological issues linked to carrier transport. The chapter ends with an overview of the possible approaches to tune the temperature coefficients of photovoltaic devices.

2.1 Definition

The concept of temperature coefficient (TC) is useful to quantify the temperature sensitivities of the performances of photovoltaic (PV) devices. In order to compare different technologies, TCs are defined normalized at 25 °C (298.15 K) (Emery et al. 1996):

O. Dupré et al., *Thermal Behavior of Photovoltaic Devices*,
DOI 10.1007/978-3-319-49457-9_2

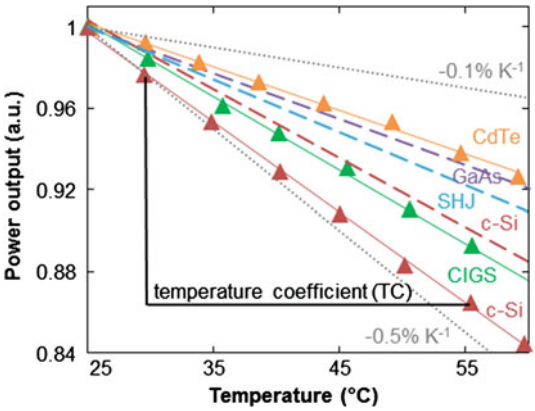

Fig. 2.1 Relative power output as a function of temperature of solar cells made of different semiconductors. Data from Siefer et al. (2005), Virtuani et al. (2010), Seif et al. (2014), Dupré et al. (2015a)

$$\beta_G(T_c) = \frac{10^6}{G(298.15\,\mathrm{K})} \frac{G(T_c) - G(298.15\,\mathrm{K})}{T_c - 298.15} \tag{2.1}$$

where G is the parameter of interest and T_c is the cell temperature. Temperature coefficients are usually expressed in ppm K^{-1} or in % K^{-1}. If variations of G are linear with temperature, β_G is well described by a single value. Conveniently, this is the case for certain important PV parameters (such as the maximum output power P_{MPP}, the open-circuit voltage V_{oc}, the short-circuit current density J_{sc} and the fill factor FF) of most types of PV cells (except a-Si cells, see Sects. 1.1.2 and 4.4, and certain other technologies such as perovskite cells, see Sect. 4.5). This is illustrated in Fig. 2.1 with the linear fits of the power outputs as a function of cell temperature for solar cells (SCs) made of different semiconductors. It is worth noticing that the efficiencies of all the PV devices shown in Fig. 2.1 decrease with increasing temperature. Also, the relative decrease rates (i.e. the temperature coefficients) are different among the semiconductors. There are also variations between devices made of the same semiconductor (e.g. c-Si in Fig. 2.1).

This chapter details the fundamental reasons for the negative temperature dependence of the photovoltaic conversion process and explains the important role of the bandgap and its temperature dependence in the thermal behavior of PV devices (Sect. 2.2). Then, Sect. 2.3 highlights the technological factors that drive the temperature coefficients of actual photovoltaic devices. Finally, Sect. 2.4 reviews the opportunities for tuning the temperature sensitivities of solar cells.

2.2 Fundamental Conversion Losses and Temperature Coefficients of Solar Cells

2.2.1 *The Detailed Balance Principle and the Thermodynamic Argument*

Fundamentally, solar cells are energy converters that take thermal energy from the Sun and turn it into electrical energy. This means that a solar cell, like any heat engine, is ultimately limited by the Carnot efficiency (which is ∼95% since the Sun's surface temperature is ∼5800 K) (Landsberg and Badescu 2000; Green 2001; Boriskina et al. 2016). However, even ideal PV devices differ from Carnot engines because the energy exchanged is radiative and because the energy emitted by the devices is considered a loss in photovoltaic conversion since the hot reservoir is the Sun (Fig. 2.2a). Moreover, typical PV cells absorb solar photons from a small solid angle while they emit in a much broader solid angle (Fig. 2.2b). Additionally, for standard single-junction cells, there is an important loss due to the spectral mismatch between the incident radiation and the absorption in the cell that generates electrical carriers (i.e. single bandgap devices absorb inefficiently the

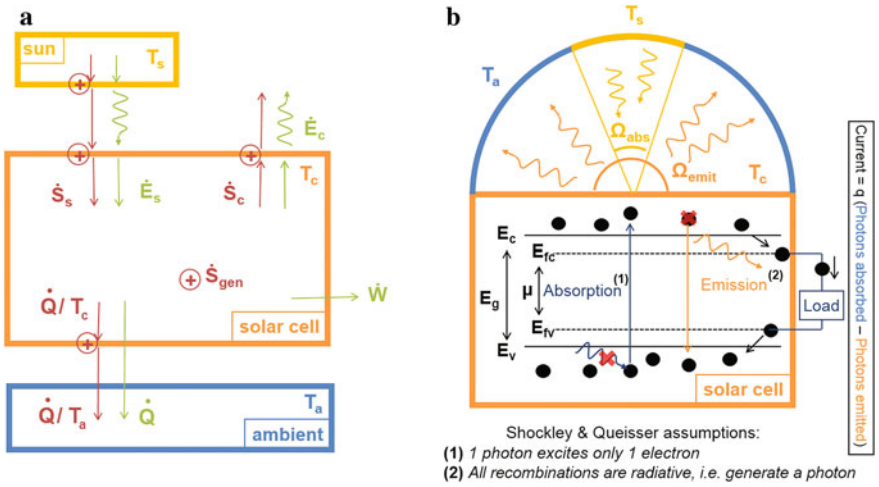

Fig. 2.2 **a** Flows of energy (in *green*) and entropy (in *red*) in and out of a solar cell. A solar cell absorbs radiative energy from the Sun with the associated entropy (see (Green 2001) for the corresponding expressions). It also emits some radiative energy with the associated entropy and evacuates some heat with the associated entropy towards the ambient. The symbol + represents the generation of entropy. The equilibrium temperature of the cell is driven by the balance between the entropy flows in and out of the cell. The power with no associated entropy flow can be converted into electrical power ($\dot{W}$); **b** Detailed balance principle illustrated with the photons fluxes in and out of a schematic solar cell. This schematic shows the direct relation that exists in the radiative limit between the populations of excited carriers and photons. It also specifies the assumptions made by Shockley and Queisser to derive their well-known efficiency limit (Shockley and Queisser 1961)

broadband incident solar spectrum). The present section illustrates how these different losses impact the conversion efficiency of PV systems.

The first assessment of the fundamental limit of photovoltaic conversion, established by Shockley and Queisser in 1961, uses the so-called detailed balance principle (Shockley and Queisser 1961). This limit, extended by several authors (Henry 1980; Tiedje et al. 1984; Araújo et al. 1994), can also be derived from a thermodynamic argument (Ross 1967; Markvart 2008). In their well-known article, Shockley and Queisser consider that all the recombinations in the solar cell are radiative, i.e. each recombination event creates a photon, and assume that each photon excites only one electron so that the population of photons and excited electrons are directly related (Fig. 2.2b). In this case, the electrical current density (J) that can be extracted from a solar cell is proportional to the difference between the rates of photon absorption (n_{abs}) and emission (n_{emit}):

$$J = q\,(n_{abs} - n_{emit}). \tag{2.2}$$

where q is the elementary charge. The source of incident photons, the Sun in the case of a solar cell, can be modeled by a blackbody at temperature T_s = 5800 K seen by the cell from a solid angle $\Omega_{abs.}$[1] It is assumed that the cell absorbs, and thus emits according to Kirchhoff's law, every photon that has at least the bandgap energy (E_g) and none that has less energy. The rate of photon absorption can be formulated by integrating Planck's equation for blackbody emission:

$$n_{abs}(E_g, T_s, \Omega_{abs}) = \frac{2\,\Omega_{abs}}{c^2 h^3} \int_{Eg}^{\infty} \frac{E^2}{\exp\left(\frac{E}{kT_s}\right) - 1} dE \tag{2.3}$$

where c is the speed of light in vacuum, and h and k are the Planck's and Boltzmann's constants, respectively.

Assuming that charge transport is perfect, the free enthalpy of the photogenerated electron-hole pairs, namely the chemical potential μ of the electron-hole system (Ruppel and Würfel 1980), is equal to qV where V is the voltage across the cell terminals. The chemical potential of the electron-hole system indicates a deviation from equilibrium. Because the system strives to come back to equilibrium, the recombination rate, which is directly linked to the emission rate in this case, increases together with the chemical potential. Considering a cell temperature T_c

[1]More precisely, here and everywhere in the present manuscript, the denomination solid angle Ω corresponds to a projection of the usual definition of the solid angle: $\int \cos\theta \, d\Omega = \int_0^{2\pi} \int_0^{\alpha} \cos\theta \, \sin\theta \, d\theta d\varphi$ (where θ and φ are the polar and azimuthal angles, respectively, and α is the angle of the cone of light) because an isotropic intensity is assumed. Note that, in normal incidence, this value is approximately equal to the solid angle if it is sufficiently small (e.g. the solid angle of the Sun seen from Earth is $6.87 \times 10^{-5} \approx \Omega_{abs} = \int \cos\theta \, d\Omega$).

and an emission solid angle Ω_{emit}[2], the photon emission rate from the cell is given by the generalized Planck's equation (Würfel 1982):

$$n_{emit}(E_g, V, T_c, \Omega_{emit}) = \frac{2\,\Omega_{emit}}{c^2\,h^3} \int_{Eg}^{\infty} \frac{E^2}{\exp\left(\frac{E-qV}{kT_c}\right) - 1} dE. \tag{2.4}$$

Equations (2.2) and (2.4) show that emission increases with the voltage V that builds in the cell and thus reduces the current that can be collected. As a consequence, there exists an optimum for the photovoltaic conversion of the radiative power incident on the cell (P_{inc}) noted η_{MPP} (MPP stands for maximum power point):

$$\eta_{MPP}(E_g, V, T_s, T_c, \Omega_{abs}, \Omega_{emit}) = \max(JV)/P_{inc}. \tag{2.5}$$

The maximum efficiency corresponds to a trade-off between current and voltage and depends on the difference between the rates of generation and recombination (in the radiative limit, the recombination rate equals the emission rate). In a given configuration (i.e. T_s, T_c, Ω_{abs}, Ω_{emit} are prescribed), the cell efficiency is only a function of E_g and V. Thus, its maximum, η_{MPP}, can be found by solving the following equations:

$$\left(\frac{\partial \eta}{\partial E_g}\right)_V = 0 \tag{2.6}$$

$$\left(\frac{\partial \eta}{\partial V}\right)_{E_g} = 0. \tag{2.7}$$

An interesting analytical solution of (2.6) can be derived by using Boltzmann's approximation[3] in (2.3) and (2.4) and calculating the integrals by parts (Hirst and Ekins-Daukes 2011):

$$q\,V_{opt} = E_g\left(1 - \frac{T_c}{T_s}\right) - k\,T_c\,\ln\left(\frac{\Omega_{emit}}{\Omega_{abs}}\right) \approx q\,V_{MPP}. \tag{2.8}$$

This analytical solution (V_{opt}) gives exactly the maximum efficiency only for the optimal E_g (i.e. when (2.7) is satisfied too) but it provides an excellent approximation of the voltage at the maximum power point (V_{MPP}) in the range of bandgaps of

[2]Note that this projected solid angle is equal to ½ of the solid angle in the case of an hemisphere (this is why usually $\Omega_{emit} = \int \cos\theta\, d\Omega = ½(2\pi) = \pi$).

[3]Photons enter the class of particles that follows Bose-Einstein statistics (these particles are called bosons). Boltzmann's approximation consists in considering the simpler Boltzmann statistics [i.e. neglecting the −1 term in the denominator of the integrand in (2.3)]. This approximation is really accurate in the range of bandgaps considered here: it is better than one part in 10^8 for $E_g > 0.5$ eV.

materials used in solar cells (Hirst and Ekins-Daukes 2011). In this equation, derived from the detailed balance principle, classical thermodynamic terms appear. The first term on the right hand side, $E_g\,(1 - T_c/T_s)$, contains the Carnot efficiency that expresses the necessity of evacuating the entropy associated with the absorbed energy flow. The second term on the right hand side, $k\,T_c\,\ln(\Omega_{emit}/\Omega_{abs})$, corresponds to the voltage loss related to the entropy generation caused by the solid angle mismatch between absorption and emission. This loss is theoretically avoidable by eliminating this solid angle mismatch. Interestingly, this can be achieved either by concentrating the incident light, i.e. increasing the solid angle of solar absorption, or by restricting the angle of emission from the device (Martí and Araújo 1996; Kosten et al. 2013, 2015). It is worth noting that these losses are function of the cell bandgap, temperature and solid angles of emission and absorption.

The current density at the maximum power point (J_{MPP}) is given by:

$$J_{MPP} = q\,(n_{abs} - n_{emit}(V_{MPP})). \tag{2.9}$$

Table 2.1 shows the analytical expressions of the energy losses related to the effects mentioned previously. The first two losses are related to the spectral mismatch between the broadband incident radiation and the restricted cell absorption: some photons have more energy than the bandgap and this "extra" energy is quickly lost by the excited electrons to the lattice atoms in a process called thermalization; some photons have less energy than the bandgap and are not able to excite any electron (sub-bandgap loss). The last three losses are driven by the balance between absorption and emission rates and thus are called "balance losses". The emission loss corresponds to the energy of the photons emitted by the PV device. The Carnot and angle mismatch losses are voltage losses associated with the emission process.

Figure 2.3a shows the fundamental losses, for single-junction solar cells under one Sun illumination, calculated as a function of bandgap energy from the analytical approximate expressions together with the exact numerical solution of the Shockley-Queisser (SQ) limit. This representation, first introduced in Hirst and Ekins-Daukes (2011), makes it straightforward to visualize the potential of different advanced PV concepts. Indeed, Fig. 2.3a highlights that the largest losses are those linked to spectral mismatch which explains the number of concepts aiming at

Table 2.1 Fundamental conversion losses in a single-junction solar cell

Spectral mismatch	Thermalization	$\frac{2\Omega_{abs}}{c^2 h^3}\int_{Eg}^{\infty}\frac{E^2}{\exp\left(\frac{E}{kT_s}\right)-1}(E - E_g)\,dE$	(2.10)
	Sub-bandgap	$\frac{2\Omega_{abs}}{c^2 h^3}\int_{0}^{E_g}\frac{E^2}{\exp\left(\frac{E}{kT_s}\right)-1}E\,dE$	(2.11)
Absorption-emission balance	Emission	$\frac{E_g}{q}\frac{2\Omega_{emit}}{c^2 h^3}\int_{E_g}^{\infty}\frac{E^2}{\exp\left(\frac{E-qV_{MPP}}{kT_c}\right)-1}\,dE$	(2.12)
	Angle mismatch	$\frac{k\,T_c}{q}\ln\left(\frac{\Omega_{emit}}{\Omega_{abs}}\right)J_{MPP}$	(2.13)
	Carnot	$\frac{E_g}{q}\left(\frac{T_c}{T_s}\right)J_{MPP}$	(2.14)

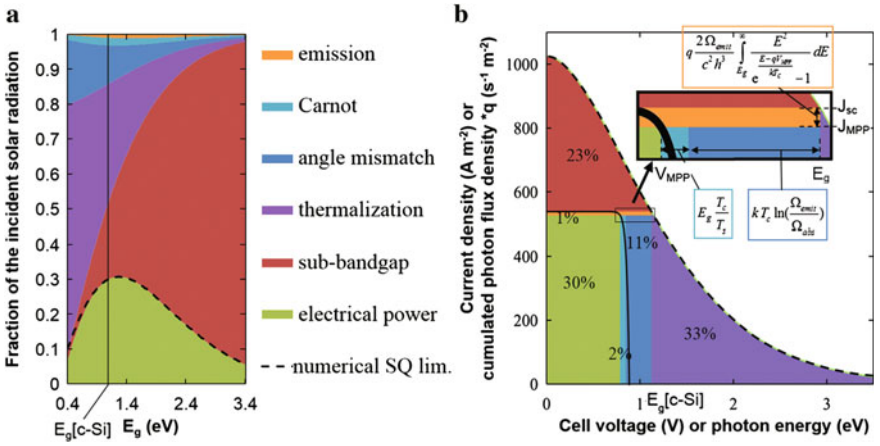

Fig. 2.3 **a** Distribution of the incident solar radiation at the optimal working point for PV conversion at 300 K under one sun illumination as a function of bandgap energy; the dashed line corresponds to the numerical solution of the Shockley-Queisser limit; **b** fundamental losses in PV conversion at the maximum power point of a c-Si PV cell at 300 K under one Sun illumination depicted together with its current-voltage characteristic

reducing these losses: hot-carrier cells (Ross and Nozik 1982; Green 2001), down conversion/multiple exciton generation (Nozik 2008; Beard 2011), intermediate band cells (Luque and Martí 1997; Brown and Green 2002; Luque et al. 2012), up conversion (Trupke et al. 2002), multi-junctions (Henry 1980), spectral splitting (Green et al. 2015), etc. Other strategies, such as concentrating sunlight (Press 1976) or limiting the cell emission angle (Kosten et al. 2013), improve the absorption-emission balance and thus reduce the angle mismatch loss (and emission as well in the "restricted angular emission" approach).

Figure 2.3b represents these fundamental loss mechanisms at the maximum power point together with the ideal current density-voltage (J-V) characteristic of a crystalline silicon (c-Si) solar cell at 300 K ($E_g \approx 1.12$ eV). The dashed line corresponds to the cumulated photon flux density plotted as a function of photon energy. The area below this line corresponds to the total power density of the incident photons. In the following, for the sake of simplicity, the term "energy" will be used instead of "power density" (energy simply corresponds to the spatial and temporal integral of power density). The different colored areas in Fig. 2.3b correspond to the different energy conversion losses in an ideal c-Si cell except for the pale green rectangle that corresponds to the electrical output energy. The dual title on the y-axis of Fig. 2.3b illustrates the relation between current and photon flux density. Indeed, each absorbed photon generates one carrier that can participate, if it does not recombine on its way, to the current that goes through the load. In short circuit, the current density, J_{sc}, is equal to the cumulated photon flux density at the bandgap because the radiative emission (and thus the recombination rate) is negligible in short-circuit condition. When the voltage of the cell increases, so does the radiative emission rate and the current drops.

The energy lost through radiative emission at the maximum power point corresponds to the number of emitted photons times their energy which is approximately equal to the bandgap energy. As for the dual title on the x-axis of Fig. 2.3b, it illustrates that the voltage of the cell is limited by the bandgap energy for standard single-junction devices.[4] Indeed, the potential energy of an excited carrier cannot exceed the energy it carries after the thermalization process because this energy loss happens much faster that the collection of excited carriers in common PV cells [in about 10^{-12} s (Würfel 2009)]. Figure 2.3b shows that the voltage at the maximum power point is lower that the bandgap because of the so-called Carnot and angle mismatch losses. These terms correspond to the minimum voltage reduction associated with radiative recombination. Indeed, any recombination process has a dual impact: a current loss because some excited charges do not make it to the external circuit; a voltage loss because the generation-recombination balance is diminished thus reducing the voltage that can build in the cell. An analogy between a PV cell and a leaky bucket feeding a water wheel is proposed in Appendix 1 to provide an intuitive understanding of the relation between the cell voltage and the generation-recombination balance. The Carnot loss corresponds to the voltage loss associated with the minimum radiative recombination rate, which happens in the radiative limit when there is no angle mismatch between radiative absorption and emission. When there is an angle mismatch, there is more emission[5] so there has to be more radiative recombination and thus a larger voltage loss, hence the angle mismatch loss term. It is important to remember that the expressions given in Table 2.1 describe only the maximum power point of the cell operation. However, it can be deduced from Fig. 2.3b how the incident energy is distributed in other $J(V)$ configurations.

The p-n junction diagram depicted in Fig. 2.4 can also help understanding the relation between the J-V curve and the different losses indicated in Fig. 2.3. In open-circuit configuration, the voltage across the cell is such that the recombination rate equals the generation rate: all the absorbed power that is not thermalized ($\sim J_{sc}\ E_g/q$) is dissipated via radiative recombinations which ultimately result in the emission of photons. In short-circuit configuration, there is no voltage across the cell so almost none of the photogenerated carriers recombine. All the absorbed power that is not thermalized is dissipated by the carrier flow through the potential drop at the junction ($\sim E_g/q$ in short circuit). At the maximum power point (MPP), there are some recombinations (current loss = emission loss term) and the voltage loss at the junction depends on the recombination rate which is driven by the cell temperature and the angle mismatch.

Figure 2.4 depicts how the energy of the incident photons is converted within an ideal p-n junction solar cell. The voltage losses can be observed on the vertical axis while the current losses are depicted by photon losses along the horizontal axis. The sub-bandgap loss represents the photons with $E < E_g$. The dashed lines show the quasi-Fermi levels of the electrons and holes. The distances between the

[4]Note that this limit can be overcome through advanced concepts such as hot-carrier cells.

[5]Kirchhoff's law of radiation dictates that $\Omega_{emit} \geq \Omega_{abs}$.

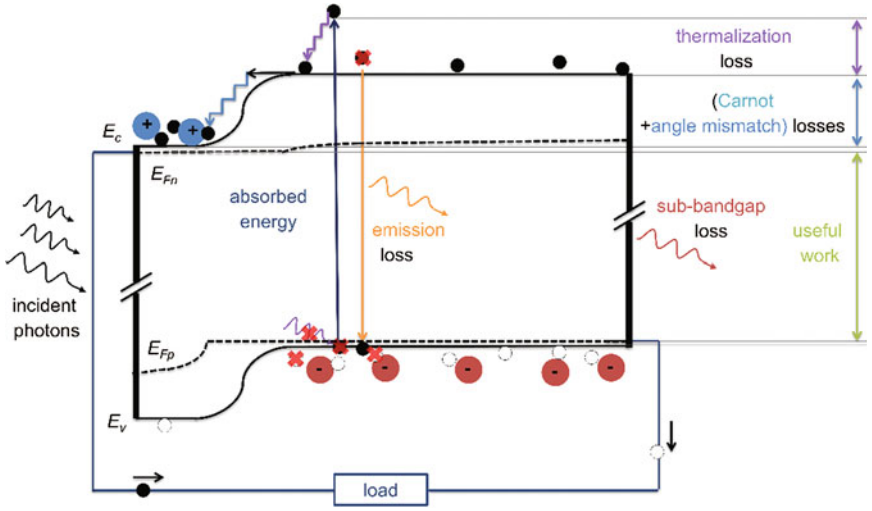

Fig. 2.4 Fundamental loss mechanisms illustrated on a p-n junction diagram. E_c and E_v are the energies of the bottom edge of the conduction band and the top edge of the valence band, respectively. E_{Fn} and E_{Fp} are the quasi-Fermi levels of electrons and holes, respectively. Figure adapted from Dupré et al. (2015b)

quasi-Fermi levels and the conduction/valence bands give an indication on the concentrations of carriers in these bands (Green 1982). This representation shows that the Carnot and angle mismatch losses occur at the p-n junction or more generally where the charges are separated (see also Fig. 2.11). This voltage loss can sometimes be split into different regions, e.g. in p-i-n junction cells. This voltage drop is necessary to efficiently collect the photogenerated charges before too many of them recombine. Physically, a fraction of their potential energy is converted into kinetic energy during the acceleration they undergo in the junction electric field. Then, they quickly relax to the potential energy of the conduction band of the other side through collisions with the lattice atoms. This heat generation process can be identified as Peltier heating (Baldasaro et al. 2001), as discussed in Chap. 3.

The fundamental losses of PV conversion being established, their dependence on temperature is the next focus. Equation (2.4) shows that radiative emission increases with cell temperature. This is the consequence of an augmentation of the recombination rate with temperature due to the increase of the equilibrium carrier concentration. This leads to a negative temperature sensitivity of the absorption-emission rate balance that is the origin of the thermal behavior of PV cells and explains why all[6] PV devices become less efficient as they heat up.

[6]Note that positive temperature coefficients have been reported for amorphous silicon and organic solar cells. However, the argument developed above holds for any kind of PV conversion device. The temperature coefficients of the aforementioned cells are expected to decrease and become negative as these technologies improve towards the radiative limit.

This conclusion can also be derived from a thermodynamical argument. Thermodynamics states that a stable system needs to have a zero net entropy balance. The energy of the solar photons comes with a certain amount of entropy (Green 2006). Thus, the photogenerated carriers need to somehow dissipate the entropy they gain upon the absorption of solar photons and possibly some additional entropy generated by parasitic processes. They do so by giving away some energy as heat, which carries entropy, to the lattice atoms. Because the flow of entropy carried by a heat flow decreases when the temperature increases, $\delta S = \delta Q/T$, equilibrating the entropy balance requires a larger loss of energy to the lattice atoms at higher temperature. This explains why the maximum PV conversion efficiency decreases as the temperature of the system increases.

The analytical expressions in Table 2.1 enable to calculate the different fundamental losses as a function of device temperature. These are plotted in Fig. 2.5 for the bandgap of c-Si at room temperature ($\sim$1.12 eV). Figure 2.5a corresponds to one Sun illumination and Fig. 2.5b to a concentration factor of 10,000. In this simplistic case, only the balance losses, i.e. emission, Carnot and angle mismatch losses, are sensitive to the cell temperature (see Table 2.1). Figure 2.5 shows that their variations with temperature are approximatively linear on the usual temperature range of solar cell operation. This explains the generally observed linear behavior of the output power of solar cells. Also, by comparing Fig. 2.5a and b, the benefit of concentrating sunlight in terms of temperature coefficient can be observed.

The analytical expressions in Table 2.1 show that the balance losses depend not only on the cell temperature but also on the semiconductor bandgap. This means that the temperature coefficient of PV conversion is fundamentally dependent upon the bandgap of the material used to absorb solar radiation. Figure 2.6 shows temperature coefficients in the radiative limit calculated as a function of cell bandgap with the analytical expressions and the full numerical calculations using the detailed balance approach. It is noteworthy that the analytical solution provides a good

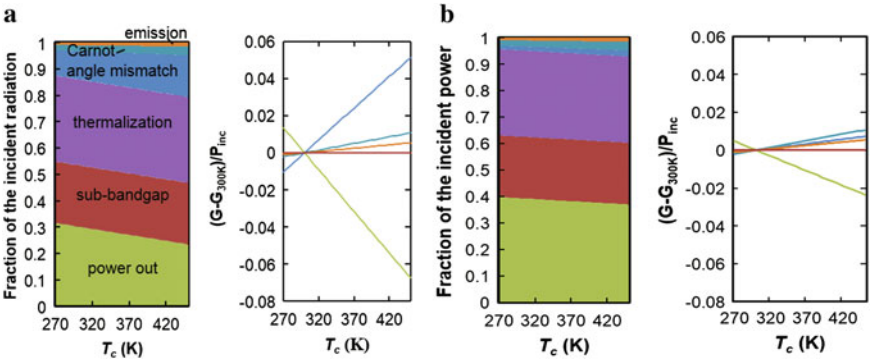

Fig. 2.5 Temperature dependence of the fundamental losses for a bandgap of 1.12 eV ($\sim E_g$(c-Si) at 298 K), **a** under one Sun illumination; **b** under 10,000 Suns. Figure adapted from Dupré et al. (2015b)

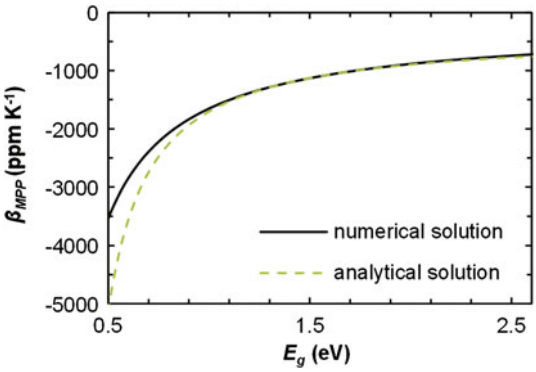

Fig. 2.6 Fundamental temperature coefficient of the maximum efficiency of single-junction solar cells as a function of bandgap

estimate of temperature coefficients as long as E_g is not too small. Also, Fig. 2.6 highlights that the absolute value of the temperature coefficient is larger for smaller bandgaps. This is due to the fact that balance losses, which increase with temperature because they originate from photon emission, are larger for smaller bandgaps (see Fig. 2.3a).

2.2.2 *Influence of Bandgap Temperature Dependence and Incident Spectrum*

All the fundamental losses in PV conversion are function of the bandgap of the material used to absorb solar radiation (see Table 2.1). The temperature coefficients plotted in Fig. 2.6 assume that bandgaps do not depend on temperature. In practice, it is well known that the bandgap of semiconductors changes substantially with temperature. This variation is due to modifications of the band energies caused by electron-phonon interactions and by thermal expansion of the lattice (Dey et al. 2013). Most semiconductor bandgaps decrease almost linearly in the temperature range of operation of solar cells (Yu et al. 2011). However, there is no general relation between bandgap and temperature dependence of bandgap as shown in Fig. 2.7.[7] Also, there are some exceptions where bandgaps actually increase with temperature. Of particular interest for photovoltaics are the perovskite[8] semiconductor compounds such as $CH_3NH_3PbI_3$ (Jiang et al. 2016), $CH_3NH_3PbI_{3-x}Cl_x$

[7]Note that there are several discrepancies for different semiconductors in the values of $E_g(T)$ reported in the literature (Varshni 1967; Pässler 1999; Vurgaftman et al. 2001).

[8]Perovskites are materials described by the formula ABX_3 where A and B are cations of different sizes (A larger than B) and X is an anion. A new class of solar cells based on mixed organic-inorganic halide perovskites (such as $CH_3NH_3PbI_{3-x}Cl_x$) has recently emerged and undergoes an extraordinary rapid development (Green et al. 2014). The inorganic counterpart $CsSnI_3$ has only achieved very low efficiency so far for reasons that are not understood yet, but also has a suitable bandgap for PV applications (Xu et al. 2014).

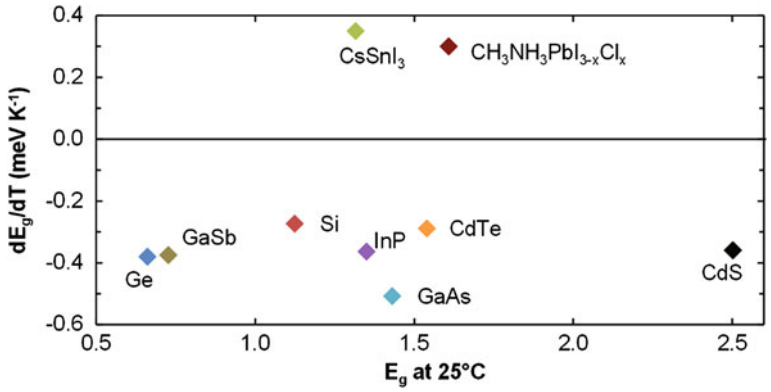

Fig. 2.7 Bandgap and slope of the linear approximation of bandgap temperature dependence around 300 K for various semiconductors. See Table 2.2 for the references

(Wu et al. 2014) or $CsSnI_3$ (Yu et al. 2011). A notable feature of perovskites is a reverse ordering of their band-edges states, i.e. their conduction band is constituted of p-like states and their valence band of s-like states (Even et al. 2012). This reverse band-edge ordering results in a bandgap temperature dependence opposite to that of tetrahedrally coordinated semiconductors (Ishihara 1994; D'Innocenzo et al. 2014; Green et al. 2014).

Since the maximum efficiency of photovoltaic conversion depends on bandgap, the temperature dependence of semiconductor bandgaps impacts directly the temperature coefficients. Also, since bandgaps vary with temperature, the spectrum of the incident radiation has an effect on the temperature coefficients. Indeed, the number of photons with energy larger than the bandgap changes with temperature as a function of bandgap variation and photon flux density. These effects are illustrated in Figs. 2.8 and 2.9. Figure 2.8 shows the Shockley-Queisser efficiency limit calculated with the AM1.5 spectrum (IEC 2008) at different temperatures with the maximum efficiencies for different semiconductors. It illustrates the different behaviors expected for the perovskites compounds whose bandgaps increase with temperature. In order to illustrate the impacts of the incident spectrum and the bandgap temperature dependences, the dashed lines in Fig. 2.9 show extrapolations of temperature coefficients as a function of bandgap assuming different values of dE_g/dT. Two extremes values of dE_g/dT (for this set of semiconductors) are used for illustration so the temperature coefficients of the materials considered are sandwiched between the dashed lines. The bumps visible on the dashed lines in Fig. 2.9 correspond to the bumps in the plots of maximum efficiency as a function of bandgap (Fig. 2.8) which originate from the irregularities in the incident AM1.5 spectrum caused by the absorption of certain molecules and Rayleigh scattering in the atmosphere (Fig. 2.10). Because of these irregularities, the impact of dE_g/dT on the maximum power temperature coefficient depends a lot on the value of the bandgap at 25 °C. Also, two semiconductors with similar bandgaps at room temperature but different dE_g/dT will ultimately, i.e. in the radiative limit, have different

thermal behaviors. For example, a PV cell made of $CH_3NH_3PbI_3$ will have a worse temperature coefficient in the radiative limit than cells made of semiconductors with a similar bandgap but a positive dE_g/dT. However, the temperature coefficients of actual solar cells depend largely on their external radiative efficiencies (see Sect. 2.3) which are already relatively high for the best perovskite solar cells to date (Green et al. 2014).

Figures 2.8 and 2.9 show that the impact of dE_g/dT on temperature coefficient is function of $d\eta/dE_g$ and thus depends on E_g and the incident spectrum. This explains

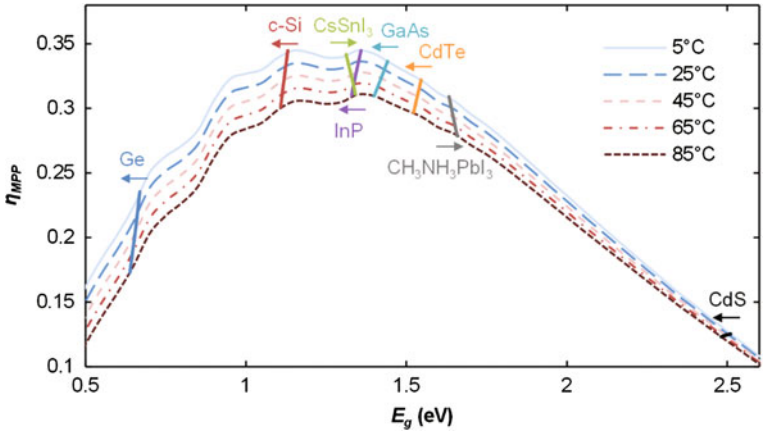

Fig. 2.8 Shockley-Queisser limit at different temperatures between 5 and 85 °C. The segments correspond to the maximum theoretical efficiencies for different semiconductors calculated using bandgap temperature dependences (references are listed in Table 2.2). Figure adapted from Dupré et al. (2015b)

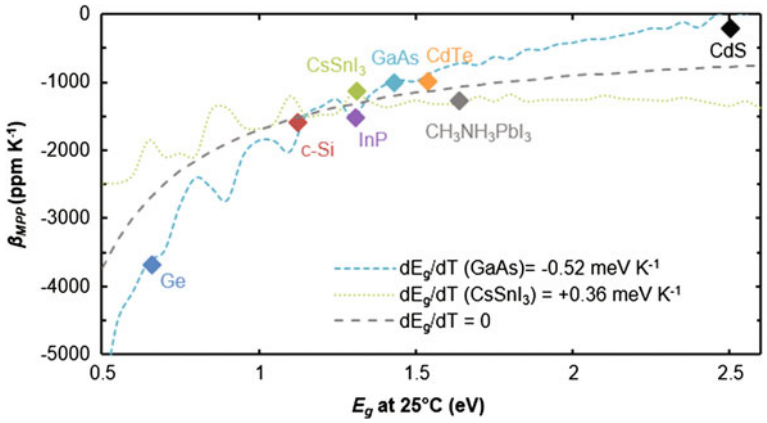

Fig. 2.9 Temperature coefficients of several semiconductors and extrapolations using different values of dE_g/dT. Figure adapted from Dupré et al. (2015b)

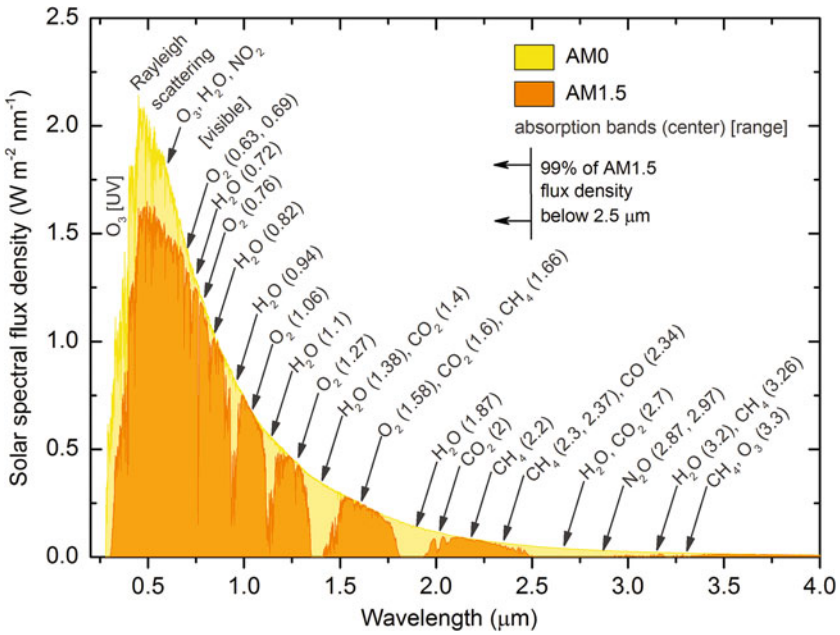

Fig. 2.10 Solar spectral flux density at the top of the atmosphere (AM0) and at sea level at a solar zenith angle of 48.19°S (AM1.5) from IEC (2008). The atmospheric absorption bands are taken from Liou (2002)

why dE_g/dT is of particular importance for semiconductors whose bandgaps are away from the optimum of the SQ limit (such as several sub-cells of multi-junction PV devices).

So far, the analysis has been derived in the radiative limit where only radiative recombinations are considered, i.e. neglecting non-radiative recombination processes such as Auger or Shockley-Read-Hall. While this situation corresponds to the ultimate efficiency of solar cells, it does not give the theoretical minima of temperature coefficients. Indeed, some of the additional losses may decrease when the temperature rises [e.g. series resistance in c-Si cells (Singh et al. 2008)]. This is the reason why unusually large or even positive[9] temperature coefficients are sometimes reported for newly-developed technologies (Green 2003). However, temperature coefficients are expected to converge towards these "fundamental"

[9]Several articles report positive temperature coefficients of the maximum power output for organic solar cells (Katz et al. 2001; Riedel et al. 2004; Ali et al. 2012). This is due to important losses at room temperature that are reduced as the temperature rises. According to Katz et al., the large TCs of cells made of conjugated polymer-fullerene composites originate from the temperature dependence of their carrier mobilities (Katz et al. 2001). Therefore the TCs of organic solar cells are expected to decrease as the technologies improve, which is the opposite of the trend of most inorganic type of solar cells.

values as technologies improve towards the radiative limit (this is illustrated for silicon cells in Fig. 2.14). To be exact, Auger recombinations[10] have to be taken into account when calculating the intrinsic limit for PV conversion of a semiconductor (Richter et al. 2013). For some semiconductors, this impacts significantly the temperature coefficients. For example, the intrinsic temperature coefficient for crystalline silicon solar cells is -2380 ppm K^{-1} while it is -1582 ppm K^{-1} in the radiative limit (Dupré 2015). This is to be compared to the values around -4500 ppm K^{-1} (0.45% $°C^{-1}$) that are common for the temperature coefficients of current commercial c-Si solar cells. The following section describes the loss mechanisms that limit the efficiency of actual PV devices and highlights those that impact their temperature coefficients.

2.3 Loss Mechanisms and Temperature Coefficients of Actual Solar Cells

Present commercial photovoltaic systems have efficiencies significantly lower than the Shockley-Queisser limit defined by the fundamental losses described previously. For example, commercial silicon solar modules on the market in 2016 have, on average, rated efficiencies of about 17% (Fraunhofer 2016) while the SQ limit for c-Si is 33.4%. Note that the record laboratory c-Si cell efficiency, which is 25.6% in July 2016 (Green et al. 2016), is getting close to the intrinsic limit efficiency of 29.43% for c-Si (Richter et al. 2013). Furthermore, the gap between the efficiency of commercial c-Si cells and the record laboratory cells is rapidly closing (Green, Sect. 2 in Boriskina et al. 2016). In this section, the additional losses limiting real device performances are introduced and their impacts on temperature coefficients are analyzed.

Figure 2.11 shows the band diagram of a realistic p-n junction solar cell operating at its maximum power point. The most important losses usually stem from the non-radiative recombinations (NRR). The different NRR processes (Shockley-Read-Hall,[11] Auger, surface[12]) are illustrated. Other losses include

[10]An Auger recombination corresponds to the crossing of an electron from the conduction band to the valence band via the transfer of some energy (at least E_g) to another electron of the conduction band. The electron of the conduction band that receives the energy quickly thermalizes back to the lower energy level of the conduction band (E_c). This process is illustrated on the p-n junction diagram in Fig. 2.11. It does not depend on defects but mainly on the local concentration of carriers, electrons and holes, in the conduction and valence bands.

[11]Shockley-Read-Hall (SRH) recombination is an extrinsic two step process by which an excited carrier recombines trough a defect state in the forbidden region (i.e. in the bandgap). Defects in the crystal lattice can have several origins such as the presence of impurities (unintentional or intentional, e.g. dopants). SRH recombination depends strongly on defect type and can have various dependences on temperature (Schenk 1992).

[12]Surfaces are regions where the lattice structure is bound to be filled with defects. Additionally, impurities tend to gather in these regions. Consequently, the bandgap is filled with defect states

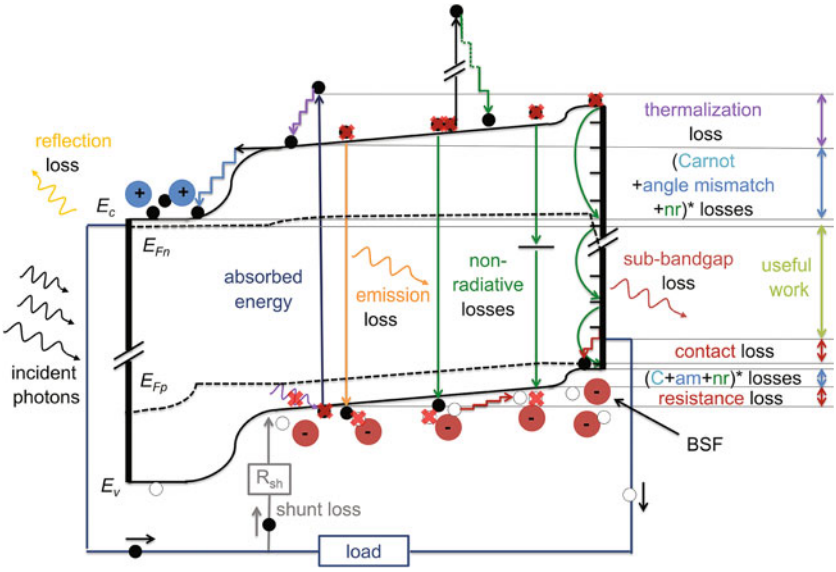

Fig. 2.11 Conversion loss mechanisms of a PV cell illustrated on a p-n junction diagram at the maximum power point. Figure adapted from Dupré et al. (2015b)

reflection at the front—illuminated side—of the cell, electrical shunts, imperfect contacts and finite mobilities of the carriers. Note that transmission losses, i.e. photons with $E > E_g$ that are not absorbed, are not depicted here but can also reduce the efficiency of thin PV cells with insufficient light trapping. The graph depicted in Fig. 2.11 is interesting in that it illustrates the different energy transformations in a solar cell. For example, it shows that the resistance loss corresponds to the kinetic energy lost by the electrical carriers to the semiconductor or metal atoms through collisions along their paths.

Similarly to Fig. 2.4, Fig. 2.11 shows that the mechanisms reducing the generation-recombination balance result in a voltage loss which occurs at the interfaces with the selective membranes that drive the photogenerated charges in opposite directions. In this example, the interfaces are the p-n junction and also the region of the back surface field (BSF) which can be seen as a p-p + junction. For other configurations, charge separation can be different (e.g. in p-i-n structures, this voltage loss is split more equally between the two separate junctions). Reflection, transmission and shunts, similarly to any current loss, also add to this voltage drop but their contribution is usually negligible so it is not depicted in Fig. 2.11 (and subsequently in Fig. 2.12). The product of the current and this potential drop

(Footnote 12 continued)

and recombinations rates are usually very high. A parameter called "surface recombination velocity" is used to quantify recombination rates at surfaces.

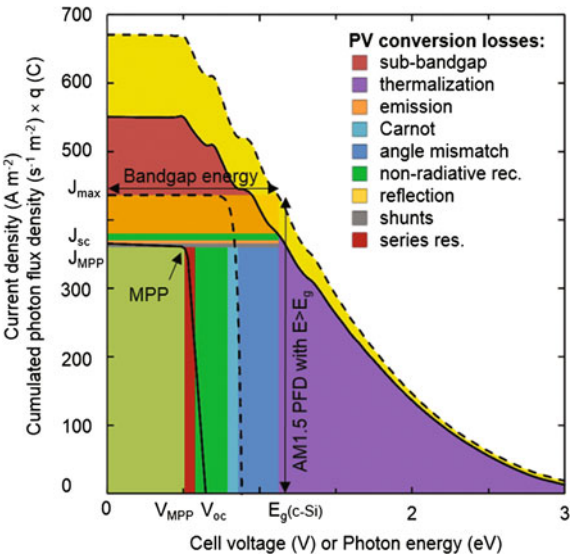

Fig. 2.12 Conversion loss mechanisms of a c-Si cell at MPP. Cumulated photon flux density of the AM1.5 spectrum (*dashed line*), of the transmitted fraction of this incident radiation perpendicularly through a planar c-Si surface (*solid line*). Ideal (*dashed line*) and actual (*solid line*) J-V characteristics of a c-Si solar cell with a planar surface. Figure adapted from Dupré et al. (2015b)

corresponds to a "collection cost": the energy required to extract the photogenerated electrical carriers from the cell before too many of them recombine.

In Fig. 2.12, the J-V curve of an illuminated c-Si cell is depicted together with the different losses at the maximum power point. Figure 2.12 shows together the cumulated photon flux density as a function of photon energy and the current density as a function of voltage (see the description of Fig. 2.3b). While Fig. 2.3b shows the cumulated photon flux density of a blackbody emission spectrum at 5800 K, Fig. 2.12 shows the cumulated photon flux density of the AM1.5 spectrum (dashed line). The full line corresponds to the cumulated photon flux density absorbed by a planar crystalline silicon cell.[13] The area between these two cumulated photon flux densities corresponds to the total energy[14] of the reflected photons. The rectangle in pale yellow illustrates the energy lost for the conversion process, i.e. the bandgap energy times the number of reflected photons with $E > E_g$. Note that the reflection loss in actual c-Si cells is much lower because of the use of anti-reflection coatings and texturization.

Figure 2.12 illustrates the different "fundamental" losses, presented in the description of Fig. 2.3b, together with the additional losses that occur in actual solar cells as described above and depicted in Fig. 2.11. As in Fig. 2.3b, by identifying the losses that limit current and voltage, it is possible to understand the shape of the J-V characteristic of a solar cell. In short-circuit configuration, there is an important current flow and no voltage across the cell: all the absorbed power is dissipated

[13]Calculated with reflectivity data from OPALv1.3 (Baker-Finch and McIntosh 2010).

[14]In this paragraph, for the sake of simplicity, "power densities" are once again replaced by "energies".

because the charges lose their potential energy to the phonons in voltage drops across the cell. In open-circuit configuration, the voltage across the cell is such that the recombination rate equals that of generation: all the power is dissipated via recombinations (non-radiative ones resulting in heat sources and a fraction of the radiative ones resulting in photon emission). The differences in heat generation in these configurations are discussed further in Chap. 3 (Sect. 3.4.1). At the maximum power point, the transport loss mechanisms come into play because there is a current flow and a voltage across the cell. Note that the dependence of the shunt and series resistances on voltage drive the slopes of the two segments of the J-V characteristic.

Since the PV cell parameters (V_{oc}, J_{sc}, FF) usually vary linearly with temperature, it is possible to separate the temperature sensitivity of a device performance into the sum of their temperature coefficients:

$$P_{MPP}(T_c) = V_{oc}(T_c)\ J_{sc}(T_c)\ FF(T_c) \tag{2.15}$$

$$\beta_{P_{MPP}} = \beta_{V_{oc}} + \beta_{J_{sc}} + \beta_{FF} \tag{2.16}$$

where P_{MPP} is the power density at the maximum power point. This is particularly interesting because these different TCs depend on different loss mechanisms. Thus, these temperature dependences provide some insight into internal device physics.

2.3.1 Open-Circuit Voltage Temperature Sensitivity

The temperature sensitivity of open-circuit voltage is of particular importance because it accounts for 80–90% of the temperature coefficient of efficiency for reasonably good solar cells (Green 2003).

The open-circuit configuration corresponds to the state where the total rate of photogeneration in the solar cell equals that of recombination so that no current circulates through the circuit. The relative change of open-circuit voltage with temperature, β_{Voc}, is thus an indication of the temperature dependence of the generation-recombination balance. The photogeneration rate is a function of incident spectrum, concentration, reflection, transmission and parasitic absorption.[15] The recombination rate depends on the type and magnitude of the recombination processes that happen in the device (radiative, SRH, Auger, surface, shunts).

The effect of temperature on PV conversion is discussed in Green's first textbook (Green 1982). The single-diode model (2.17) is used with a general expression of the diode saturation current density (2.18) and the temperature dependence of

[15]Parasitic absorption corresponds to the absorption by the lattice atoms or by free carriers of potentially useful photons, i.e. with $E \geq E_g$. These absorption mechanisms prevent the creation of electron-hole pairs and result in the generation of heat (see Sect. 3.2).

short-circuit current is neglected to express the temperature sensitivity of open-circuit voltage mainly as a function of bandgap and open-circuit voltage (2.19). The corresponding equations read:

$$J \approx J_{sc} - J_0 \exp\left(\frac{qV}{kT_c}\right) \tag{2.17}$$

$$J_0 = A\, T_c^{\gamma} \exp\left(-\frac{E_{g0}}{kT_c}\right) \tag{2.18}$$

$$\frac{d\,V_{oc}}{dT_c} = -\frac{\frac{E_{g0}}{q} - V_{oc} + \gamma\frac{kT_c}{q}}{T_c} \tag{2.19}$$

$$E_{g0} = E_g - T_c \frac{dE_g}{dT_c} \tag{2.20}$$

where A is a factor independent of temperature, E_{g0} is the bandgap of the semiconductor linearly extrapolated to 0 K, and γ includes the temperature dependences of several parameters which determine the diode saturation current density J_0.

Appendix 2 describes the origin of this expression of the diode saturation current, (2.18), that is used with different semi-empirical parameters in many works dealing with temperature coefficients (Fan 1986; Landis 1994; Yoon and Garboushian 1994; Friedman 1996). In short, the γ term accounts for the temperature dependences of several parameters such as the number of effectively available states in the conduction and valence bands, carrier mobilities and lifetimes (which depend on the dominant recombination mechanisms), etc. An interesting discussion on the physical meaning of the parameter J_0 can be found in Cuevas (2014).

Equation (2.19) shows the important relation between the open-circuit voltage and its temperature sensitivity. It predicts an approximately linear temperature dependence of the open-circuit voltage and shows that the temperature coefficient of V_{oc} should decrease as V_{oc} increases. In Green et al. (1982), it is mentioned that "as the open-circuit voltage of silicon solar cells continues to improve, one resulting advantage, not widely appreciated, is reduced temperature sensitivity of device performance". This is an important understanding which is verified experimentally as illustrated in Fig. 2.13 for c-Si solar cells. Note that it is generally valid for all kinds of PV devices.

The parameter γ in (2.19) is not directly related to device physics, which can lead to systematic errors in modeling as demonstrated in Green (2003). In this article, a general analysis of the temperature behavior of a PV cell based on internal device physics is proposed. The temperature dependence of open-circuit voltage is shown to be mainly driven by the recombination mechanisms which depend on the excess carrier concentrations. As a matter of fact, Shockley-Read-Hall, Auger and radiative recombination rates can be written as a function of the product of the electron and hole carrier concentrations (np). This np product depends on the intrinsic carrier

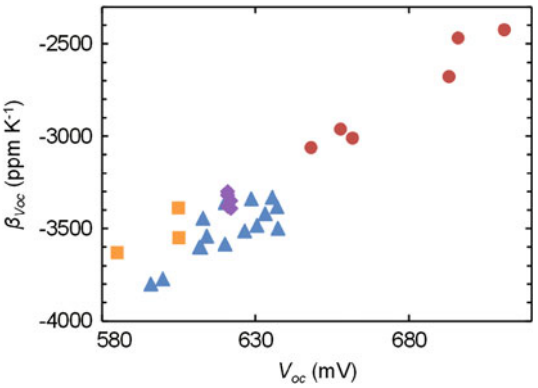

Fig. 2.13 Experimental temperature coefficient of the open-circuit voltage of c-Si solar cells as a function of open-circuit voltage. *Data sources* Triangles from Ponce-Alcántara et al. (2014), squares from Xiao et al. (2014), diamonds from Tanay et al. (2011) and circles from Green et al. (1982, 1985 and Zhao et al. (1994)

concentration, n_i, and on the splitting of the quasi-Fermi levels, E_{Fp}–E_{Fn}, which is related to the potential, V, in the cell:

$$np = n_i^2 \exp\left[\frac{q\,(E_{Fp} - E_{Fn})}{k\,T_c}\right]. \tag{2.21}$$

For convenience, the term ξ, closely related to the np product, is introduced:

$$\xi = np\,\exp\left(-\frac{E_g}{k\,T_c}\right)/n_i^2. \tag{2.22}$$

Regardless of the recombination mechanisms, the output current of a cell (I) can be written as the photogenerated current, I_L, minus the sum of the different recombination processes:

$$I = I_L(V, T_c) - \sum_{i=1}^{N} A_i(V) T_c^{\gamma_i} f_i(\xi_i) \tag{2.23}$$

where the terms $A(V)$ and T^{γ} accommodate for second-order additional dependences on temperature and voltage which can originate from parameters such as diffusion lengths, surface recombination velocities, depletion region width, etc. Using (2.23) in open-circuit configuration and differentiating gives (Green 2003):

$$\frac{dV_{oc}}{dT_c} = -\frac{\left(\frac{\langle E_{g0}\rangle}{q} - V_{oc} + \frac{kT_c}{q}\left\langle \gamma \frac{f}{\xi}\frac{d\xi}{df}\right\rangle - \frac{kT_c}{qI_L}\frac{dI_L}{dT}\left\langle \frac{f}{\xi}\frac{d\xi}{df}\right\rangle\right)}{T_c\left(1 + \frac{kT_c}{q}\left\langle \frac{1}{A}\frac{dA}{dV}\frac{f}{\xi}\frac{d\xi}{df}\right\rangle - \frac{kT_c}{qI_L}\frac{\partial I_L}{\partial V}\left\langle \frac{f}{\xi}\frac{d\xi}{df}\right\rangle\right)} \tag{2.24}$$

where <*G*> is the weighted value of the parameter of interest defined as:

$$\langle G \rangle = \frac{\sum_{i=1}^{N} G_i A_i T_c^{\gamma_i} \xi_i \left(df_i / d\xi_i \right)}{\sum_{i=1}^{N} A_i T_c^{\gamma_i} \xi_i \left(df_i / d\xi_i \right)}. \tag{2.25}$$

Neglecting the second-order terms in (2.24), the temperature sensitivity of open-circuit voltage can then be written simply as:

$$\frac{dV_{oc}}{dT_c} = -\frac{\left(\frac{\langle E_{g0} \rangle}{q} - V_{oc} + \frac{kT_c}{q} \left\langle \gamma \frac{f}{\xi} \frac{d\xi}{df} \right\rangle \right)}{T_c}. \tag{2.26}$$

This expression is similar to (2.19) but the term $<\gamma \frac{f}{\xi} \frac{d\xi}{df}>$ provides a direct link to the underlying physics. The expressions (2.24) and (2.26) can be applied to any kind of PV cell as they are derived from perfectly general arguments but they require the detailed knowledge of the dominant recombination mechanisms.

It is possible to derive another similar expression for the temperature sensitivity of open-circuit voltage using the concept of external radiative efficiency (ERE). The ERE of a PV cell is similar to the external quantum efficiency (EQE) of a light-emitting diode (LED). It is defined as "the fraction of the total dark current recombination in the device that results in radiative emission from the device" (Green 2012). Note that the ERE is different from the ratio of radiative recombination rate on total recombination rate, which is the internal radiative efficiency (IRE), because of photon recycling. Indeed, only a fraction of the photons emitted through radiative recombinations actually exits the cell (see for example Fig. 3.2). Using the definition of the ERE, the output current and the open-circuit voltage of the cell can be written as (Dupré et al. 2015b):

$$\begin{aligned} J &= X J_{sc,1sun} - \frac{1}{ERE} J_{0,rad} \left(\exp\left(\frac{qV}{kT_c} \right) - 1 \right) \\ &\approx X J_{sc,1sun} - \frac{1}{ERE} J_{0,rad} \exp\left(\frac{qV}{kT_c} \right) \end{aligned} \tag{2.27}$$

$$V_{oc} = \frac{kT_c}{q} \ln\left(\frac{X J_{sc,1sun}}{(1/ERE_{oc}) J_{0,rad}} \right) = V_{oc,1sun} + \frac{kT_c}{q} \left(\ln(ERE_{oc}) + \ln(X) \right) \tag{2.28}$$

where $J_{sc,1sun}(T_c) = q \int_{E_g(T_c)}^{\infty} PFD\,(E)\,dE$, ERE_{oc} is the ERE at open circuit, X is the concentration factor and $J_{0,rad}$ is the dark current density in the radiative limit. Transport resistances are neglected. Writing $X\,J_{sc,1sun}$ instead of J_{sc} means that a linear behavior of J_{sc} with the concentration factor X is assumed. This assumption

can fail if an important loss mechanism in short circuit has a significant intensity dependence. Nonetheless, (2.28) shows that increasing the concentration factor generally improves open-circuit voltage and in turn improves its temperature coefficient. A specific discussion about concentrator PV devices is presented in Sect. 4.7.

Similarly to concentration, the effect of non-ideal absorption could easily be included in (2.28) and (2.30) through the collection fraction f_c (see Sect. 2.3.2). However, in practice, its impact on the temperature coefficient of open-circuit voltage is limited (e.g. a collection fraction increase from 60 to 80% causes only 2.6% change in β_{Voc}).

The dark current density in the radiative limit can be written as[16]:

$$J_{0,rad} \approx q \frac{2\,\Omega_{emit}}{c^2\,h^3} k\,T_c\,E_g^2\,\exp\left(-\frac{E_g}{k\,T_c}\right). \tag{2.29}$$

Assuming a linear variation of E_g on the temperature range of interest, $E_g = E_{g0} + T_c\,\frac{dE_g}{dT_c}$, and differentiating (2.28), the temperature dependence of V_{oc} reads (Dupré et al. 2015b):

$$\frac{dV_{oc}}{dT_c} = -\frac{\frac{E_{g0}}{q} - V_{oc} + \gamma\frac{kT_c}{q}}{T_c} \tag{2.30}$$

with:

$$\gamma = 1 - \frac{d\ln ERE_{oc}}{d\ln T_c} + \left(2\frac{d\ln E_g}{d\ln T_c} - \frac{d\ln J_{sc,1sun}}{d\ln T_c}\right). \tag{2.31}$$

The expression (2.30) is the same as (2.19) but the coefficient γ is explicitly quantified in (2.31). It corresponds to the temperature sensitivity of the mechanisms determining V_{oc}, similarly to the term $\left\langle \gamma\frac{f}{\xi}\frac{d\xi}{df}\right\rangle$ in (2.26). One advantage of using the concept of external radiative efficiency, is that it enables to compare solar cells of both the same and completely different technologies (Green 2012). Making the rough approximations of neglecting the temperature dependences of ERE and bandgap, Fig. 2.14 shows temperature coefficients as a function of cell bandgap for different external radiative efficiencies. This gives an idea of the evolution of temperature coefficients as cells improve towards the radiative limit. For example, the crosses in Fig. 2.14 correspond to experimental values of β_{Voc} for record-efficiency crystalline silicon cells over the years. Note that the relation between *ERE* and β_{Voc} is not so straightforward because ERE and bandgap temperature dependences are not always negligible. Figure 2.15 illustrates that dE_g/dT

[16]This expression is derived from Planck's equation using Boltzmann's approximation and neglecting $2E_gkT + 2k^2T^2$ in front of E_g^2 in the integration by parts (Dupré 2015).

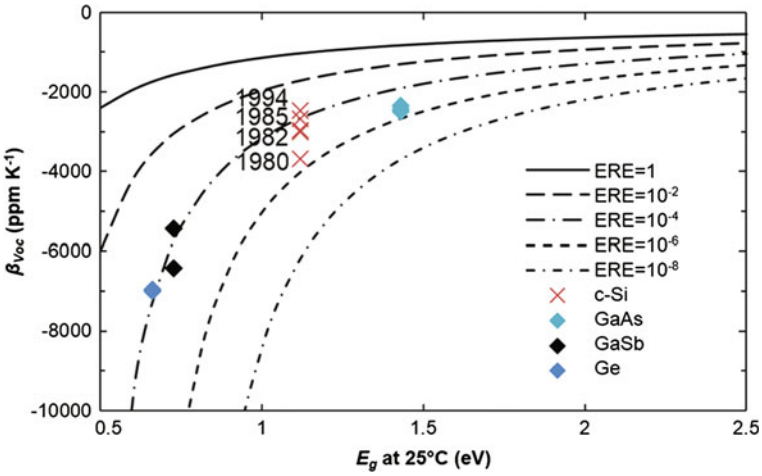

Fig. 2.14 Temperature coefficient of open-circuit voltage as a function of bandgap for different values of the external radiative efficiency (dE_g/dT and $dERE/dT$ are neglected in the calculation). The crosses are experimental values of β_{Voc} for some record-efficiency c-Si cells over the years (Green et al. 1982, 1985; Zhao et al. 1994). The diamonds are experimental values of β_{Voc} for GaAs, GaSb and Ge cells (Siefer et al. 2005). Figure adapted from Dupré et al. (2015b)

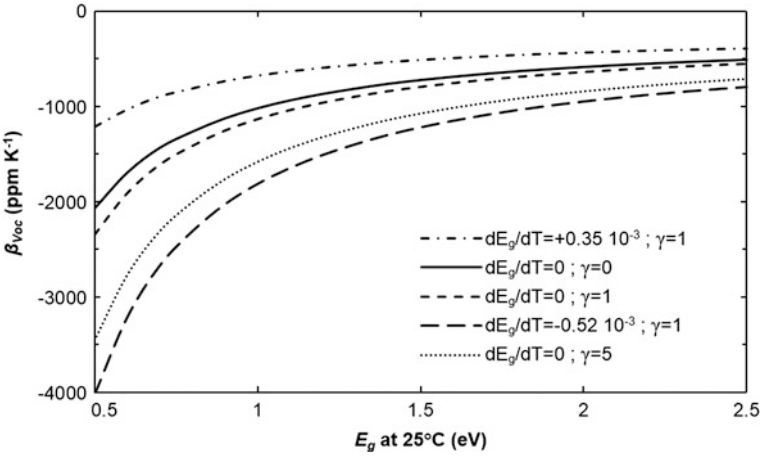

Fig. 2.15 Temperature coefficient of open-circuit voltage as a function of bandgap for $ERE = 1$ and different values of dE_g/dT and γ. Figure from Dupré et al. (2015b)

and γ can have a significant impact on β_{Voc}. The value of γ depends on $dERE/dT$ which is function of the dominant recombination mechanisms. Consequently, the knowledge of V_{oc} or ERE at 25 °C alone is not sufficient to accurately predict β_{Voc}.

The absolute value of the terms in parentheses in (2.31) is usually less than 0.5 (Dupré 2015). Thus, it is $1 - d\ln ERE_{oc}/d\ln T_c$ that plays a major role in the value

of γ. Since the temperature dependence of ERE is function of the recombination mechanisms within the cell, the parameter γ contains an information on the dominant recombination processes. This idea can be illustrated by analyzing two situations where the saturation current is dominated by different recombination mechanisms (Siefer and Bett 2012). The starting point is the single-diode model using the diode ideality factor, n, and the dark saturation current density J_0:

$$J = J_{sc} - J_0\left(\exp\left(\frac{qV}{nkT_c}\right) - 1\right) \approx J_{sc} - J_0 \exp\left(\frac{qV}{nkT_c}\right). \tag{2.32}$$

The open-circuit voltage then reads:

$$V_{oc} \approx \frac{nkT_c}{q} \ln\left(\frac{J_{sc}}{J_0}\right). \tag{2.33}$$

- Scenario 1: the dominant recombination mechanism is recombination through defects (Shockley-Read-Hall) in the bulk regions and at the surfaces. In this case, recombination rates are only limited by minority carrier concentrations and the ideality factor is equal to one. The dark saturation current density can be written as (Green 1982):

$$J_{01} = q\left(\frac{D_e}{L_e}\frac{1}{N_A}F_P + \frac{D_h}{L_h}\frac{1}{N_D}F_N\right) n_i^2 \tag{2.34}$$

where F_P and F_N are factors that account for the finite dimensions of the P and N regions respectively (and are thus function of the surface recombination velocities). $D_{e,h}$ and $L_{e,h}$ are the diffusion coefficients and the diffusion lengths of electrons and holes. $N_{A,D}$ are the doping concentration of acceptors and donors respectively and n_i is the intrinsic carrier concentration. Neglecting the temperature dependence of $D_e/L_e\ F_P$ and $D_h/L_h\ F_N$, the temperature dependence of J_0 comes only from n_i^2. The square of the intrinsic carrier concentration reads (Sze and Ng 1981):

$$\begin{aligned} n_i^2 &= N_c N_v \exp\left(-E_g/kT_c\right) \\ &= 4\left(2\pi k T_c/h^2\right)^3 \left(m_e\, m_h^*\right)^{3/2} \exp\left(-E_g/kT_c\right). \end{aligned} \tag{2.35}$$

Neglecting the temperature dependence of the electron and hole effective masses, m_e^* and m_h^*, it follows that:

$$n_i^2(T_c) \propto T_c^3 \exp\left(-E_g(T_c)/kT_c\right). \tag{2.36}$$

Thus:

$$J_{01}(T_c) \propto T_c^3 \exp\left(-\frac{E_g(T_c)}{kT_c}\right). \tag{2.37}$$

Using (2.37) in the derivation of (2.33) gives:

$$\frac{dV_{oc}}{dT_c} = -\frac{\frac{E_{g0}}{q} - V_{oc} + \frac{kT_c}{q}\left(3 - \frac{d\ln J_{sc}}{d\ln T_c}\right)}{T_c}. \tag{2.38}$$

Equation (2.38) corresponds to (2.30) with $\gamma = 3 - \frac{d\ln J_{sc}}{d\ln T_c} \approx 3$.

- Scenario 2: the dominant recombination mechanism is recombination through defects (Shockley-Read-Hall) in the depletion zone. In this case, the recombination rate is limited by both minority and majority carrier concentrations and the ideality factor is equal to two. The dark saturation current density can be written as (Siefer and Bett 2012):

$$J_{02} = \frac{n_i\, W_d\, k\, T_c}{2(V_d - V)\tau_{n0}} \tag{2.39}$$

where W_d is the width of the depletion zone, V_d is the diffusion voltage also known as built-in voltage and τ_{n0} is the minimum electron lifetime. Neglecting the temperature dependence of these parameters and using (2.36) gives:

$$J_{02} \propto T_c^{2.5} \exp\left(-\frac{E_g(T_c)}{2kT_c}\right). \tag{2.40}$$

Using (2.40) in the derivation of (2.33) results in:

$$\frac{dV_{oc}}{dT_c} = -\frac{\frac{E_{g0}}{q} - V_{oc} + \frac{kT_c}{q}\left(5 - 2\frac{d\ln J_{sc}}{d\ln T_c}\right)}{T_c} \tag{2.41}$$

which corresponds to (2.30) with $\gamma = 5 - 2\frac{d\ln J_{sc}}{d\ln T_c} \approx 5$.

These scenarios illustrate the impact of the dominant recombination mechanisms on γ and correspondingly the information contained in this parameter. Of course, there exist other recombination mechanisms that have different temperature dependences such as Auger or radiative recombination. For example, in the radiative limit (*ERE* = 1), (2.31) gives $\gamma \approx 1.2$ for crystalline silicon. Also, it is possible that, in some cases, the assumptions made in the two scenarios presented above (neglecting the temperature dependence of the carrier lifetime or the surface recombination velocity for example) do not hold, leading to different values for γ.

Besides, in actual devices, several mechanisms with different temperature and voltage dependences often contribute to the global recombination rate. In this case, the J-V characteristic has to be modeled with a double (or more) diode model and it becomes complicated to derive an analytical expression of dV_{oc}/dT_c using the same approach. Instead of using the diode model, Grover et al. propose another formulation of solar cell physics that enables to assess quantitatively the strengths of the different possible recombination pathways from simple J-V measurements on a range of temperatures and intensities (Grover et al. 2013). Quite similarly to the derivation in Green (2003), the recombination rates and the open-circuit voltage are expressed as a function of a parameter ς closely related to the *np* product:

$$V_{oc} = \frac{kT_c}{q}\ln\left(\frac{np}{n_i^2}\right) = \frac{kT_c}{q}\ln\left(\varsigma^2\right). \tag{2.42}$$

Expressing that the total generation rate in the cell is equal to the recombination rate at open circuit gives:

$$\left(R_0^I + R_0^I\right)\varsigma^2 + R_0^I\varsigma = \int_W G_x dx = G_{avg}W \tag{2.43}$$

where G_{avg} is the total generation rate divided by the cell thickness, W, and R_0^b, R_0^d and R_0^I correspond to the strengths of the recombination mechanisms independent of bias conditions (respectively in the bulk, the depletion region and at the interfaces). These parameters R_0 carry the same physical meaning as the parameters usually denoted J_0 in the diode models.

Solving (2.43) gives the following expression of the open-circuit voltage:

$$V_{oc} = 2\frac{kT_c}{q}\ln\left[k_1\left(\sqrt{1 + k_2 G_{avg}} - 1\right)\right] \tag{2.44}$$

with:

$$k_1 = \frac{R_0^d}{2\left(R_0^I + R_0^b\right)}; \quad k_2 = 4W\frac{\left(R_0^I + R_0^b\right)}{\left(R_0^d\right)^2}. \tag{2.45}$$

This set of equations contains the temperature and intensity dependence of V_{oc} and shows the dependence of V_{oc} on the different recombination processes via R_0^b, R_0^d and R_0^I. Thus, it is possible to use this theoretical framework to identify and quantify different recombination pathways in PV devices using simple electrical measurements (i.e. temperature and intensity dependent J-V measurements). With this method, it is possible to extract valuable information on device physics as demonstrated for silicon heterojunctions, CIGS, C_uO_2 and GaAs solar cells in Grover et al. (2013), Li et al. (2014a, b), Grover and Li (2015).

While the analytical method presented above can provide useful insights into device physics, it often requires some prior knowledge of the device considered. Another approach consists in fitting temperature and intensity dependent V_{oc} measurements to a complete 1-D drift-diffusion model (Brandt et al. 2016). This type of numerical modelling associated with simple electrical measurements may be an interesting alternative to longer and more costly spectroscopy studies in the ongoing search for new materials for PV applications.

2.3.2 Short-Circuit Current Temperature Sensitivity

The short-circuit current density, J_{sc}, generally increases slightly with temperature. This is mainly due to the fact that most semiconductor bandgaps decrease with temperature (see Fig. 2.7). The short-circuit current density depends on the number of photons able to create an electron-hole pair, i.e. with $E > E_g$, and on the loss mechanisms in short circuit such as parasitic absorption or surface recombination for example. Thus, J_{sc} can be expressed as the product of an ideal short-circuit current density $J_{sc,ideal}$ and a collection fraction f_c (Green 2003):

$$J_{sc} = J_{sc,ideal} f_c. \tag{2.46}$$

The ideal short-circuit current density is determined by the photon flux density (PFD) of the incident radiation and the cell bandgap:

$$J_{sc,ideal}(T_c) = q \int_{E_g(T_c)}^{\infty} PFD\,(E)\,dE. \tag{2.47}$$

The temperature dependence of $J_{sc,ideal}$ depends on the temperature dependence of the bandgap. If the bandgap decreases when temperature rises, more electron-hole pairs can potentially be photogenerated and $dJ_{sc,ideal}/dT_c$ is positive. For semiconductors such as perovskites whose bandgaps increase with temperature, the temperature dependence of $J_{sc,ideal}$ is negative.

The temperature coefficient of the short-circuit current can be written as (Green 2003):

$$\beta_{J_{sc}} = \frac{1}{J_{sc}}\frac{dJ_{sc}}{dT_c} = \frac{1}{J_{sc,ideal}}\frac{dJ_{sc,ideal}}{dE_g}\frac{dE_g}{dT_c} + \frac{1}{f_c}\frac{df_c}{dT_c} \tag{2.48}$$

The collection fraction f_c is the fraction of potentially useful photons ($E \geq E_g$) that excites a carrier that gets collected in short circuit. It accounts for optical losses such as reflection, insufficient or parasitic absorption as well as electrical losses such as bulk or surface recombination that happen in short-circuit condition. It is closely related to the external quantum efficiency (EQE) and can be expressed as:

$$f_c(T_c) = \frac{J_{sc}(T_c)}{J_{sc,ideal}(T_c)} = \frac{q\int_0^\infty EQE(E)\,PFD\,(E)\,dE}{q\int_{E_g(T_c)}^\infty PFD\,(E)\,dE} \tag{2.49}$$

The expression (2.48) of the temperature coefficient of J_{sc} is interesting in that it separates the influence of intrinsic material properties from that of device parameters. The first summand is a function of the solar cell material (its bandgap and its bandgap temperature sensitivity) and the intensity and spectrum of the irradiation. The second summand is related to the cell light trapping ability and collection efficiency. It can be derived from external quantum efficiency (EQE) measurements on a range of temperatures.

The first summand in (2.48) indicates that β_{Jsc} depends on the incident spectral intensity at wavelengths near the bandgap. Figure 2.16 shows the photon flux density of the reference AM1.5 spectrum (IEC 2008) and that of a solar simulator (Emery 2008) together with the bandgaps of several semiconductors at 0 and 100 °C. While the average intensity of solar simulators is close to that of the reference spectrum, the photon flux densities can be quite different as illustrated in Fig. 2.16. This explains the scattering of β_{Jsc} values in the literature (Landis 1994). Even for indoor measurements, the spectral intensity distributions vary between different solar simulators (even of the same type). This stresses the complexity of accurately predicting β_{Jsc} under real operating conditions, where the incident spectrum changes over time.

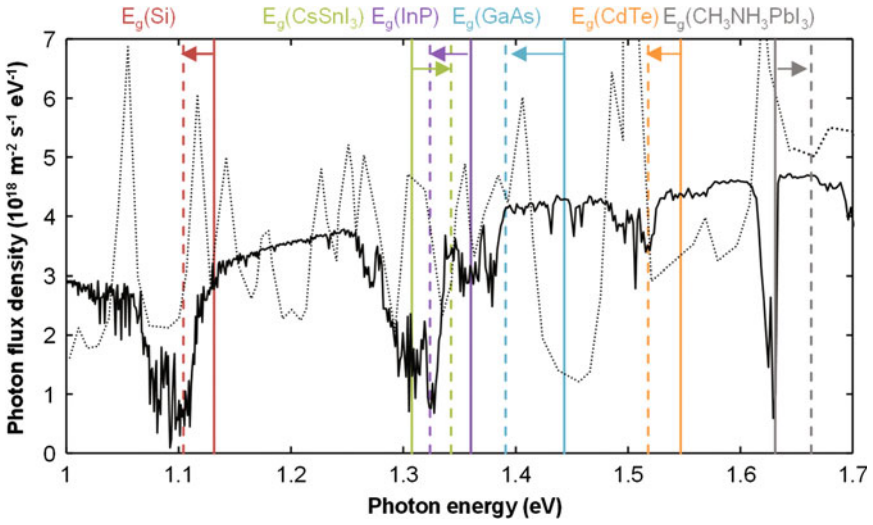

Fig. 2.16 Photon flux density of the AM1.5 reference spectrum (*solid line*), of a solar simulator (Emery 2008) (*dotted line*). Bandgaps of different semiconductors at 0 and 100 °C (shown by *solid* and *dashed lines* respectively); the *arrows* show the direction of increasing temperature. Figure adapted from Dupré et al. (2015b)

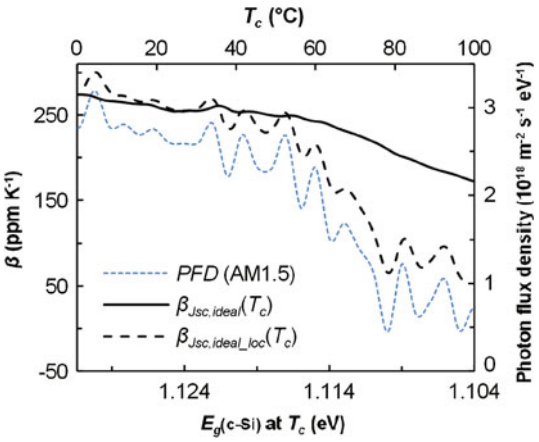

Fig. 2.17 Global (*solid line*) and local (*dashed line*) temperature coefficients of the short-circuit current density of a c-Si cell with ideal light collection (f_c = 1). Photon flux density of the AM1.5 reference spectrum (*dotted line*). Figure adapted from Dupré et al. (2015b)

Figure 2.16 shows that some semiconductor bandgaps lie near important fluctuations in the AM1.5 photon flux density. This induces non-linearity in the temperature dependence of the ideal short-circuit current density. Figure 2.17 illustrates this phenomenon in the case of c-Si. The temperature coefficient of short-circuit current density undergoes a change of 37% between 0 and 100 °C. This variation can be related to the photon flux density fluctuations. To represent the local variations of $J_{sc,ideal}$, a local temperature coefficient ($\beta_{G,loc}$) is defined (in ppm K^{-1}) as:

$$\beta_{G,loc}(T_c) = \frac{10^6}{G(298.15\,\mathrm{K})} \frac{G(T_c+1) - G(T_c-1)}{2} \tag{2.50}$$

Figure 2.17 shows that the local variations of the ideal short-circuit current density are proportional to the local variations of the photon flux density. This illustrates the impact of the photon flux density on the temperature coefficient of the short-circuit current density.

The first summand in (2.48) accounts for the change in the number of photons with $E > E_g$ caused by the temperature dependence of the bandgap. This term explains the difference in β_{Jsc} between cells based on different semiconductors. For example, using dE_g/dT from Table 2.2 and the photon flux density of the AM1.5 spectrum, this term is equal to about 250, 460, 670 and -450 for c-Si, GaAs, CdTe and $CH_3NH_3PbI_3$ respectively.

The temperature coefficients of the short-circuit current density of actual devices can differ from these values because of the second summand in (2.48) which accounts for non-idealities. In general, the collection fraction increases with temperature and $1/f_c \times df_c/dT_c$ is positive. Note that this term is usually larger for indirect bandgap materials because phonons play an important role in their interband absorption. The positive temperature dependence of interband absorption results in an interesting trend for c-Si cells: β_{Jsc} tends to decrease when J_{sc} increases (Fig. 2.18). One possible explanation is that, regardless of the loss mechanism, the

Table 2.2 Bandgaps of various semiconductors at room temperature and values of dE_g/dT from linear fits around 300 K

Semiconductor	E_g @ 25 °C (eV)	dE_g/dT (meV K^{-1})	Source for $E_g(T)$
c-Si	1.125	−0.27	Green (1990)
Ge	0.661	−0.38	Varshni (1967)
GaAs	1.431	−0.51	
InP	1.351	−0.36	
CdTe	1.540	−0.29	Singh and Ravindra (2012)
CdS	2.503	−0.36	
GaSb	0.727	−0.38	Vurgaftman et al. (2001)
$CH_3NH_3PbI_3$	1.639	0.32	Jiang et al. (2016)
$CH_3NH_3PbI_{3-X}Cl_X$	1.608	0.30	Wu et al. (2014)
$CsSnI_3$	1.316	0.35	Yu et al. (2011)

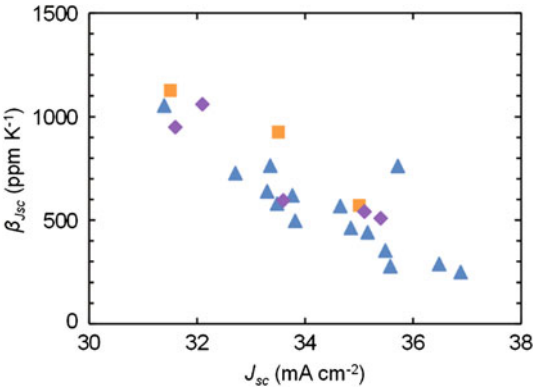

Fig. 2.18 Experimental temperature coefficients of short-circuit current density as a function of short-circuit current density. *Data sources*: *Triangles* from Ponce-Alcántara et al. (2014), *squares* from Xiao et al. (2014) and *diamonds* from Tanay et al. (2011)

cells that collect less electron-hole pairs at room temperature benefit relatively more from the increased absorption with temperature. This effect is illustrated in Fig. 2.19 where the gain in EQE when the temperature increases from 25 to 40 °C is highlighted for two c-Si cells with different short-circuit current densities. Because the cell with a low EQE collects less of the potentially useful photons at room temperature, it undergoes a larger boost in EQE, and thus in collection fraction, when the temperature rises. Note that the trend apparent in Fig. 2.18 is not a general rule and devices with different light trapping structures can present different trends (Dupré 2015).

Similarly to the temperature coefficient of V_{oc}, that of J_{sc} contains information on some of the loss mechanisms in the solar cell. To obtain some insight into the physics of carrier collection, it is interesting to analyse the variations with temperature of the external quantum efficiency. In Philipps et al. (2011), a numerical model including the temperature dependences of material parameters (e.g. bandgap)

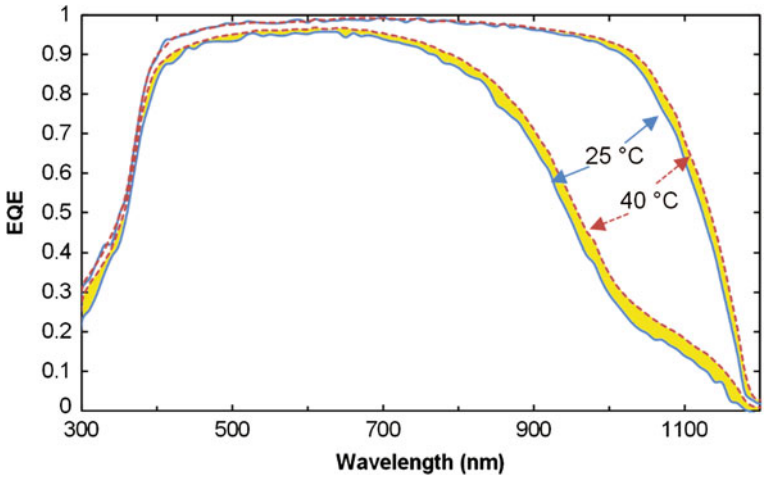

Fig. 2.19 EQEs at 25 and 40 °C (*solid* and *dashed lines* respectively) of two c-Si cells. The variations of EQE between 25 and 40 °C are highlighted. Figure created with data from Dupré et al. (2015a)

and physical processes (e.g. recombination rates) is used to extract information from measurements of the EQE of GaAs cells over a range of temperature. The analysis enables a better understanding of the thermal behavior of these cells. Another example of the use of temperature dependent EQE measurements can be found in Søndenå et al. (2015). The EQEs from compensated and non-compensated polysilicon cells are compared and the different changes with temperature are associated with differences in minority carrier lifetimes and mobilities of the bulk materials.

2.3.3 Fill Factor Temperature Sensitivity

The fill factor (*FF*) relates the maximum power that can be extracted from a cell (P_{MPP}) to the product of its open-circuit voltage (V_{oc}) and short-circuit current (I_{sc}). It indicates the minimal "cost" of extracting the photogenerated charges from the cell into the circuit and corresponds to the optimal current/voltage trade-off. This optimum depends on the generation-recombination balance (similarly to V_{oc}) but also on the transport losses associated with the current flow through the circuit at the maximum power point (MPP).

When both series and shunt resistances have a negligible impact on cell performance, the fill factor can be accurately expressed as (Green 1981):

$$FF_0 = \frac{v_{oc} - \ln(v_{oc} + 0.72)}{v_{oc} + 1} \tag{2.51}$$

where v_{oc} is the normalized open-circuit voltage defined as:

$$v_{oc} = \frac{n\,k\,T_c}{q}\,V_{oc} \tag{2.52}$$

where n is the diode ideality factor. Assuming that the ideality factor and series and shunt resistances do not vary significantly with temperature, the temperature coefficient of the fill factor can be approximated as (Green et al. 1982):

$$\beta_{FF_0} = \frac{1}{FF_0}\frac{dFF_0}{dT_c} \approx (1 - 1.02\,FF_0)\left(\frac{1}{V_{oc}}\frac{dV_{oc}}{dT_c} - \frac{1}{T_c}\right) \tag{2.53}$$

This expression highlights the relation between β_{FF} and β_{Voc}, which results from the fact that the fill factor also depends upon the generation-recombination balance in the cell. Note that (2.53) neglects the effect of parasitic transport losses.

When the series resistance, R_s, is important and the shunt resistance is so large as to have a negligible effect, the fill factor is better described by Green (1981):

$$FF_s = FF_0\left(1 - \frac{R_s}{V_{oc}/I_{sc}}\right). \tag{2.54}$$

The temperature coefficient of the fill factor becomes (Zhao et al. 1994):

$$\beta_{FF} = \frac{1}{FF}\frac{dFF}{dT_c} \approx (1 - 1.02\,FF_0)\left(\frac{1}{V_{oc}}\frac{dV_{oc}}{dT_c} - \frac{1}{T_c}\right) - \frac{R_s}{V_{oc}/I_{sc} - R_s}\left(\frac{1}{R_s}\frac{dR_s}{dT_c}\right). \tag{2.55}$$

In this expression, certain transport losses appear in the second summand. This term can be significant especially in early, non-optimized, devices. Even in the case of a record efficiency PERC cell, this second summand is 303 ppm K^{-1} which corresponds to 25% of the total temperature coefficient of the fill factor (Zhao et al. 1994). While (2.55) takes into account series resistance, it has been observed that it does not accurately predict the fill factor temperature sensitivity of certain solar cells (Dupré et al. 2015a). The discrepancies between the measurements and the values of β_{FF} predicted by (2.55) may be due to variations with temperature of the ideality factor and the shunt resistance which are neglected in the derivation of (2.55). These effects are particularly important in certain devices. For example, in certain amorphous silicon and nanocrystalline dye cells, the fill factor increases with temperature (which is the opposite of the usual trend) due to decreasing resistance effects or increasing "mobility-lifetime" products (Green 2003; Riesen et al. 2016). It is also interesting to note that the impact of series resistances

generally increases with irradiance because of the augmentation of current circulating through the cell (Helmers et al. 2013). Similarly, the effect of shunt resistance is more important at low illumination levels. Additionally, certain limiting transport mechanisms cause important non-linearities in β_{FF} which result in non-linear β_η (see Sects. 4.2 and 4.4).

An interesting example of the relation between the limiting transport mechanisms and the temperature coefficient of the fill factor in CIGS modules is reported in Deceglie et al. (2014). The temperature coefficient of the fill factor of CIGS modules is found to be increased after light soaking. It is suggested that this is due to a light induced reduction in the conduction band offset between the buffer and the absorber. Since thermionic emission is the limiting charge transfer mechanism across this barrier and it increases with temperature (Sze and Ng 1981), this metastable change could explain the observed variation of β_{FF}. In other words: the decrease of interface resistance with temperature depends upon the height of the barrier that carriers have to go through. Light soaking modifies this barrier height and thus impacts the temperature coefficient of the fill factor. This understanding is important because it is the final light soaked temperature coefficients that need to be known in order to predict field performances.

Another example of the impact of transport barriers on the temperature sensitivity of the fill factor is highlighted in Seif et al. (2014) for silicon heterojunction (SHJ) cells. In this work, the intrinsic amorphous silicon layer at the front is replaced by an amorphous silicon oxide layer in order to reduce optical losses. However, at room temperature, the gain in short-circuit current is more than compensated by a loss in fill factor. This loss in fill factor is attributed to a valence band offset impeding the collection of holes. The effect of this transport barrier decreases with temperature because, unlike standard devices which operate in a carrier-diffusion-limited regime, the limiting charge transfer mechanism here is thermionic emission of the carriers across the barrier. Once again, this transport barrier whose effect decreases with temperature results in a more favorable temperature coefficient of the fill factor. This effect of transport barriers on β_{FF} are also reported in SHJ cells when using thicker amorphous silicon layers (Taguchi et al. 2008) or a MoOx hole selective contact (Battaglia et al. 2014). Additionally, the results in Seif et al. (2016) suggest that the thermal behavior of SHJ cells is impacted not only by transport-related phenomena but also by the passivation properties of the interfaces.

In Seif et al. (2014), the advantageous β_{FF} of the device with the amorphous silicon oxide layer results in a better β_η which translates into better performances than the standard device at temperatures above 45 °C. This result demonstrates that there exist opportunities to tune the temperature coefficients of solar cells and optimize their designs at their operating temperature instead of at 25 °C (which is the temperature prescribed in the standard test conditions, see Sect. 3.5).

2.4 Tuning the Temperature Coefficients

While the importance of temperature coefficients for the energy yield of PV devices is well known (it is even advertised by several PV manufacturers), the idea of tuning the temperature coefficients is seldom mentioned in the literature. It is now understood that temperature coefficients generally improve together with open-circuit voltage so that improved temperature sensitivity automatically follows from ameliorations in V_{oc}. This explains, for example, the advantageous temperature coefficients of silicon heterojunction solar cells also known as HIT[17] cells (see Sect. 4.2). Another illustration of the positive impact of open-circuit voltage is the reduced temperature coefficients of PV systems operating under concentration (e.g. Yoon and Garboushian 1994). Note that while PV systems under concentration have reduced temperature sensitivities, the increased incoming irradiance also results in an increased heat generation in the device (see Sect. 4.7). Interestingly, the concept of reduction of the angle of emission should theoretically improves temperature sensitivity (see Sect. 2.2.1) without increasing the incoming power and thus the heat source, making this solution ideal in terms of thermal behavior. However, thermal behavior and temperature coefficients are rarely considered as design parameters of PV devices. Furthermore, as discussed in the previous sections, open-circuit voltage is not the only factor that influences the temperature sensitivities of a PV device performances.

The main driver of the temperature coefficient of the efficiency of a solar cell is its bandgap energy (see Sect. 2.2). This is why, in general, cells made of large bandgap materials such as GaAs or CdTe have better temperature coefficients than that those made of c-Si for example. Also, each semiconductor has a specific bandgap temperature dependence caused by electron-phonon interactions and by thermal expansion of the lattice (see Sect. 2.2.2). Depending on the value of the bandgap at room temperature, the bandgap temperature dependence (dE_g/dT) can affect either positively or negatively the temperature sensitivity of PV conversion efficiency. Figure 2.8 illustrates that, for an AM1.5 illumination, cells with bandgaps larger than $\sim$1.5 eV benefit, in terms of temperature coefficient, from negative dE_g/dT while cells with bandgaps lower than $\sim$1.5 eV benefit from positive dE_g/dT (such as that of perovskite compounds). Several articles indicate that the bandgap temperature sensitivities of certain quantum dots (QD) change with their size (Olkhovets et al. 1998; Dey et al. 2013). This highlights a potential way of tuning dE_g/dT to optimize the temperature coefficients of QD solar cells. Another way of adjusting dE_g/dT could be via mechanical stress. For example, in ultra-thin micro-transfer printed cells, the thermal expansion of the substrate impacts the

[17]HIT stands for Heterojunction with Intrinsic Thin layers. This kind of silicon heterojunction solar cells consists of a layer of c-Si, which serves as the absorber, sandwiched between two very thin layers (few nanometers) of amorphous silicon with different doping, which serve as selective membranes. These layers are separated by very thin layers of excellent quality amorphous silicon which passivate the interfaces and enable high open-circuit voltages.

thermal expansion of the lattice of the cell active layer and thus modifies dE_g/dT (Menard et al. 2012). Other ways to modify a semiconductor bandgap include doping at high concentration [effect known as bandgap narrowing (Sze and Ng 1981)] and applying an hydrostatic pressure (Goni et al. 1990).

The previous sections have highlighted that temperature coefficients of solar cells depend on the temperature dependences of all the limiting loss mechanisms. This suggests that the temperature coefficients of a device can be tuned by modifying its design. For example, in the case of space applications, it is suggested in Landis (1994) that it could be worth improving the open-circuit voltage at the expense of performances at 25 °C (by increasing base doping of the cell for example) to reduce the temperature sensitivity of the devices. Ideally, this could lower the temperature-related losses and lead to better performances in real operating conditions. Another example can be found in Seif et al. (2015) where it is proposed that the temperature coefficient of the fill factor can be tuned by adding layers that impede carrier transport at room temperature. In Riesen et al. (2016), the effect of several design parameters of a-Si:H solar cells (i-layer thickness, H_2/SiH_4 flow ratio, etc.) on J-V parameters and their temperature coefficients is studied experimentally. The results highlight the impact of cell design on its thermal behavior and thus on energy yield. This work also shows that an optimum cell design depends on the range of operating temperature which originates from the operating conditions (climate of the location, mounting configuration, etc.).

The potential of tuning the temperature coefficients in order to optimize a solar cell so that it performs better at its actual operating temperature is demonstrated in Seif et al. (2014). In this work, a new cell design, while less efficient in the standard test conditions, is shown to outperform the standard design above a certain temperature thanks to an advantageous temperature coefficient. This means that the device with the highest efficiency in the STC do not necessarily provide the highest energy output. This idea is illustrated in Fig. 2.20 with the results mentioned above (Seif et al. 2014). The efficiency of the SHJ cell with the original feature (an amorphous silicon oxide layer) is plotted in green and the efficiency of the standard SHJ cell is plotted in orange. As mentioned, the modified cell design underperforms at 25 °C but benefits from an advantageous temperature coefficient which translates into better performances than the standard device at temperatures above 45 °C. The bar charts in Fig. 2.20 represent the distribution of annual energy production as a function of module temperature in Norway (blue bars) and in the US desert Southwest (red bars). It appears that, in the US desert Southwest, more than 50% of the annual energy production is generated when the module temperature is above 45 °C. This means that the modified SHJ cell design would have a better energy yield in this location than a standard SHJ cell (but not if it was installed in Norway). This demonstrates that there exist opportunities to tune the temperature coefficients of solar cells and optimize their designs as a function of their operating temperature instead of at 25 °C. This concept of thermal design of PV devices is discussed further in Chap. 3, Sect. 3.5.

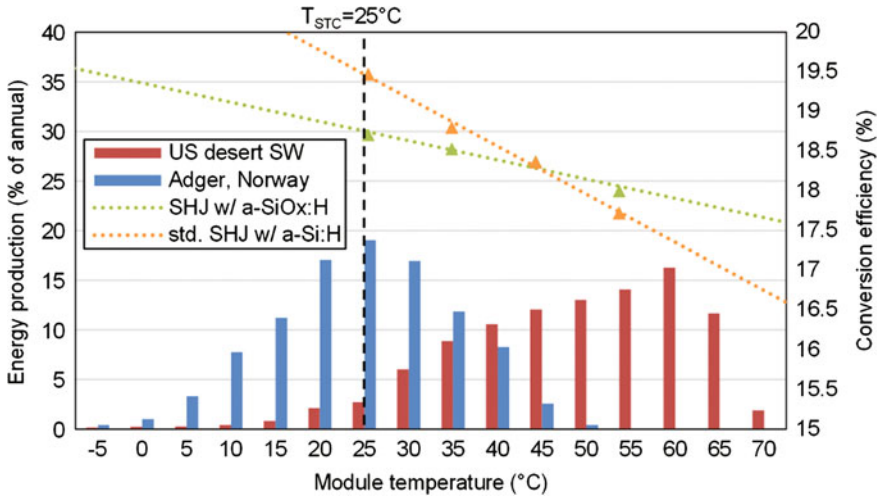

Fig. 2.20 Distribution of annual energy production as a function of module temperature in Norway (*blue bars*) and in the US desert SouthWest (*red bars*). Conversion efficiency as a function of device temperature of a standard SHJ cell (*orange dots*) and a SHJ cell with an amorphous silicon oxide windows layer (*green dots*). Data from Strevel et al. (2012), Seif et al. (2014) and data provided by the Energy Materials Group at the University of Agder (Norway)

2.5 Conclusion

The efficiency of photovoltaic conversion is fundamentally dependent upon the converter temperature. This temperature dependence is negative and its magnitude depends upon the bandgap of the PV device. In general, solar cells made of larger bandgap semiconductors have lower temperature sensitivities. In addition, bandgap temperature dependence, which varies among different materials, modifies the temperature sensitivities as a function of the radiative spectrum incident upon the device.

To these intrinsic effects, add several extrinsic effects dues to non-idealities in existing devices. Each loss mechanism in a solar cell has a specific voltage and temperature dependence. Therefore, the temperature dependence of certain solar cell parameters (V_{oc}, J_{sc}, FF) which correspond to different bias configurations (open circuit, short circuit, MPP) can provide some information about the dominating loss mechanisms.

In open-circuit configuration, the total recombination rate is equal to the total generation rate. Thus, the open-circuit voltage is a function of the different recombination processes that happen in the device. The temperature dependence of open-circuit voltage can be used to identify and quantify the dominant recombination pathways by their functional dependences.

In short-circuit configuration, the current depends on the photogeneration of electron-hole pairs and on the efficiency at which they are collected. The

photogeneration depends on the incident spectrum and the bandgap as well as on the optical design of the device. The temperature dependence of the photogeneration mainly comes from that of the bandgap of the absorbing material. On the other hand, the temperature dependence of the collection fraction gives some indication about the loss mechanisms responsible for the incomplete absorption or collection of the available photons. In general, this term is larger for indirect bandgap materials such as c-Si because their interband absorption coefficients increase with temperature.

The fill factor, which links P_{MPP} to V_{oc} and J_{sc}, depends on the generation-recombination balance at MPP which is usually related to the generation-recombination balance in open circuit, hence a relation between β_{FF} and β_{Voc}. At the maximum power point, there is a current flowing through the device so the fill factor is also a function of the limiting transport mechanisms.

The temperature coefficients of PV devices are function of a large number of parameters that can be tuned by design. There exist several opportunities for optimizing the temperature dependences of PV devices performances. While some of them come naturally with improvements in V_{oc} for example, other approaches consist in optimizing the performances in specific operating conditions at the expense of the performances in the standard test conditions.

Appendix 1

Analogy Between a Photovoltaic Cell and a Leaky Bucket Feeding a Water Wheel

The analogy illustrated in Fig. 2.21 is inspired by a lecture from Prof. Yablonovitch at the International School of Solid State Physics in 2012. The version presented here is modified to explain better certain physical mechanisms of solar cell operation. In this analogy, a photovoltaic device is compared with a leaky

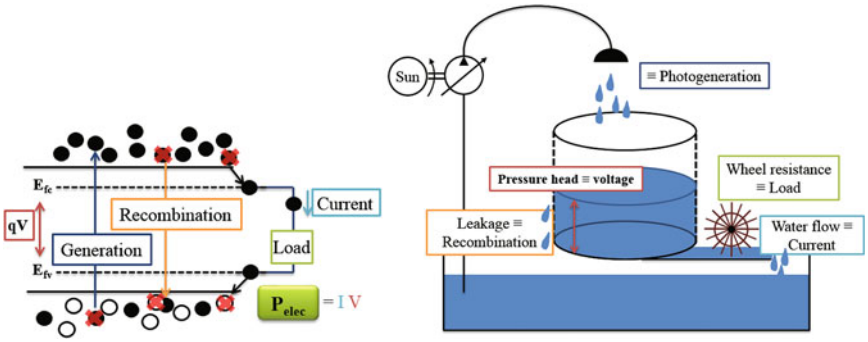

Fig. 2.21 Hydraulic analogy of the operating principles of a solar cell

bucket of water. This leaky bucket is connected to a water wheel whose mechanical resistance represents the electrical resistance of the load connected to the solar cell. The power dissipated in the wheel (≡output power) is equal to the product of the water flow, analog of the electrical current, and the pressure head in the bucket which compares to the voltage across the solar cell. Water flows into the bucket by a hose connected to a pump powered by the Sun. The water droplets represent the electrons excited into the conduction band by the incident solar photons. The bucket leaks through its sidewalls to represent the recombination of excited carriers. The more water is in the bucket, the more water leaks from the sides just like recombination rates increase when the cell voltage increases. This analogy illustrates that the amount of water in the bucket (≡cell voltage) depends on the balance between water flowing in by the hose (≡photogeneration) and water flowing out by its sides or through the water wheel (≡recombination and output current). To transfer the maximum power into the wheel, its resistance needs to be adjusted so that it is not too low to maintain some pressure in the bucket but not too high to prevent excessive leaking from the bucket. When the resistance of the waterwheel is negligible—short-circuit configuration—the bucket does not fill and most of the water entering through the shower head exits directly through the waterwheel ($J_{sc} \approx J_{photogenerated}$). When the outlet to the waterwheel is closed—open-circuit configuration—the bucket fills with water until the flow leaking through the sides equals that entering from the shower head. This explains why the open-circuit voltage indicates the balance between photogeneration and recombination rates.

Appendix 2

Temperature Dependence of the Diode Saturation Current

The following expression is often used for the diode saturation current density of a solar cell (Green 1982):

$$J_0 = C\,T^{\gamma} \exp\left(-\frac{E_{g0}}{k\,T_c}\right). \tag{2.56}$$

This expression is fundamental as it is a basis for many works dealing with temperature coefficients (Fan 1986; Nell and Barnett 1987; Landis 1994; Yoon and Garboushian 1994; Friedman 1996). The diode saturation current density, J_0, is a fundamental parameter of solar cells. It corresponds to the diffusion current density of carriers in the reverse diode direction when no voltage is applied, i.e. it is the diffusion current density that balances the drift current density at the p-n junction in equilibrium (Fig. 2.22a). Under an applied forward bias V, the potential at the junction is lowered and the concentration of carriers with enough energy to diffuse

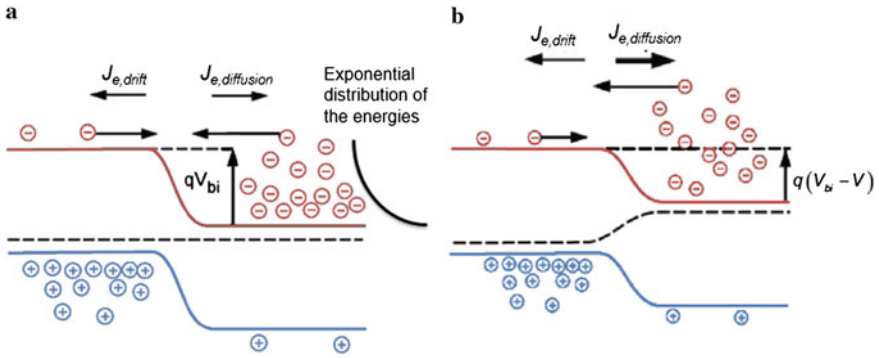

Fig. 2.22 p-n junction diagram in the dark under **a** no bias, **b** an external bias *V*. Figure adapted from a document by Bill Wilson under a Creative Commons Attribution License http://cnx.org/contents/8c8d95ff-8ac8-421c-a009-6bff6b862903@14/P-N_Junction:_Part_I

across it, is increased by $\exp(qV/kT_c)$ (Fig. 2.22b). This explains the form of the ideal diode law (Shockley 1948):

$$J = J_0 \left(\exp\left(\frac{q\,V}{k\,T_c} \right) - 1 \right). \tag{2.57}$$

The principle of superposition states that for a linear system, the response to several excitations is equal to the sum of the responses caused by each individual excitation. In the case of a solar cell, the excitations can be caused by light and/or voltage. Assuming linearity (which is usually valid under low injection conditions, i.e. when majority carrier concentrations are much larger that minority carrier concentrations), the principle of superposition states that the current density that can be extracted from a solar cell (J) equals that photogenerated (J_{ph}) minus that recombined which corresponds to the current density flowing in reverse bias through the diode in the dark:

$$J = J_{ph} - J_0 \left(\exp\left(\frac{q\,V}{k\,T_c} \right) - 1 \right) \tag{2.58}$$

This expression illustrates the name commonly given to the parameter J_0 (diode or dark saturation current density). Indeed, in the dark and under a large reverse bias, the current saturate towards the value J_0. However, the parameter J_0 has a more profound physical signification: it is proportional to the recombination rate in thermal equilibrium (with no applied bias). It is used to describe the strength of the recombination mechanisms independent of the bias condition. Because the value of the bias corresponds to the magnitude of the disequilibrium, the recombination rate can often be written as the product of J_0 and $\exp(qV/kT_c)$. However, the situation can be more complex because different recombination mechanisms have different

bias dependences. There is an interesting discussion on the physical meaning of the parameter J_0 and an analysis of different recombination scenarios in Cuevas (2014).

Under a number of assumptions (detailed in Green 1982), J_0 can be derived easily from the carrier transport equations:

$$J_0 = q\left(\frac{D_e}{L_e}\frac{1}{N_A}F_P + \frac{D_h}{L_h}\frac{1}{N_D}F_N\right)n_i^2 \tag{2.59}$$

F_P and F_N are factors that account for the finite dimensions of the P and N regions of a pn junction solar cell respectively and are thus function of the surface recombination velocities. $D_{e,h}$ and $L_{e,h}$ are the diffusion coefficients and the diffusion lengths of electrons and holes. $N_{A,D}$ are the doping concentrations of acceptors and donors. n_i is the intrinsic carrier concentration which is maybe the most crucial parameter in cell modeling. It corresponds to the concentration of carriers that are thermally excited from the valence band to the conduction band in an intrinsic, i.e. non-doped, material. For a non-degenerate semiconductor, i.e. where the Fermi energy is at least $3kT_c$ away from either band edge, the product of the electron and hole intrinsic concentrations is given by Green (1982):

$$n_i^2 = N_c N_v \exp(-E_g/kT_c) \tag{2.60}$$

where N_c and N_v are the number of effectively available states in the conduction and valence bands.

Comparing (2.56) with (2.59) and (2.60) shows that the term γ describes the temperature dependence of a large number of parameters (namely N_c, N_v, F_P, F_N, D_e, D_h, L_e, L_h, N_A and N_D).

The densities of states can be calculated by solving the Schrödinger equation assuming the simple particle-in-a-box model. Using the Boltzmann probability function (instead of the Fermi-Dirac probability function in the case of a non-degenerate semiconductor), the product of effectively available states in the conduction and valence bands, N_c and N_v, can be written as:

$$N_c N_v = 4\,(2\,\pi\,k\,T_c/h^2)^3 (m_e^* m_h^*)^{3/2} \tag{2.61}$$

where m_e* and m_h* are the effective masses of the electrons and the holes.

F_P and F_N are temperature dependent because of the temperature dependence of the surface recombination velocities.

The diffusion coefficients D_e, D_h are related to the carrier mobilities by the Einstein relations:

$$D_{e,h} = \mu_{e,h}\frac{k\,T_c}{q}. \tag{2.62}$$

The thermal energy kT_c which causes the random motion of carriers is logically present in the equation of the diffusion coefficient. Also, the mobilities of the

carriers are function of temperature. These temperature dependences are function of the doping concentrations because doping impacts the carrier equilibrium concentrations (Klaassen 1992a, b).

The diffusion lengths (L_e, L_h) correspond to the average distances traveled by excited carriers before their recombination. They depend on the diffusion coefficients (D_e, D_h) and the lifetimes of the carriers (τ_e, τ_h):

$$L_{e,h} = \sqrt{D_{e,h}\tau_{e,h}}. \tag{2.63}$$

Lifetimes are also temperature dependent because the different existing recombination mechanisms are function of the cell temperature (Huldt et al. 1979; Schenk 1992; Trupke et al. 2003).

Eventually, the dopant concentrations, N_A and N_D, may depend on temperature in the case of incomplete ionization of the dopants in the range of temperature of interest.

The number of temperature dependent parameters listed above illustrates the complexity of the temperature dependence of the diode saturation current density. In several works (e.g. Nell and Barnett 1987; Friedman 1996), the temperature dependence of $\frac{D_e}{L_e}\frac{1}{N_A}F_P$ in (2.59) is neglected and it is assumed that the temperature dependence of J_0 is driven only by that of n_i^2 (neglecting possible temperature dependences of the effective masses). This gives:

$$J_0 = C\,T_c^3 \exp\left(-\frac{E_{g0}}{k\,T_c}\right) \tag{2.64}$$

where C is a constant assumed independent of the temperature.

Additional parameters are sometimes used in the diode saturation current density equation (Fan 1986; Yoon and Garboushian 1994). For example, the following equation, initially proposed by Fan, is the basis for several works on temperature coefficients (Fan 1986):

$$J_0 = C\,T_c^{3/a} \exp\left(-\frac{E_g}{b\,k\,T_c}\right) \tag{2.65}$$

where C is an empirical parameter related to the cell material and a,b are "empirical parameters depending on the quality of the cell material and junction" (Fan 1986). These parameters are sometimes extracted from fits to experimental data and are not directly correlated to any physical mechanism. However, such analyses can lead to systematic errors in the modeling (Green 2003).

It is noteworthy that the expression of the diode saturation current given by (2.59) corresponds to a scenario where recombinations mainly occur in the quasi-neutral regions, i.e. in the bulk, or at the surfaces. There exist several expressions derived for different limiting scenarios. For example, if the

recombinations are mostly happening in the depletion region, the diode saturation current can be written as (Siefer and Bett 2012):

$$J_{02} = \frac{n_i W_d k T_c}{2(V_d - V)\tau_{n0}} \tag{2.66}$$

where W_d is the width of the depletion zone, V_d is the diffusion voltage and τ_{n0} is the minimum electron lifetime. This expression shows a different temperature dependence from (2.59). A discussion of different possible scenarios is presented in Sect. 2.3.1.

References

Ali B, Murray R, Hegedus SS, Ismat Shah S (2012) Analysis of voltage and temperature dependent photocurrent collection in P3HT/PCBM solar cells. J Appl Phys 112:1–11. Doi:10.1063/1.4768910

Araújo GL, Martí A (1994) Absolute limiting efficiencies for photovoltaic energy conversion. Sol Energy Mater Sol Cells 33:213–240. Doi: 10.1016/0927-0248(94)90209-7

Baker-Finch SC, McIntosh KR (2010) A freeware program for precise optical analysis of the front surface of a solar cell. In: 35th IEEE photovoltaic specialists conference (PVSC). IEEE, pp 2184–2187

Baldasaro PF, Raynolds JE, Charache GW et al (2001) Thermodynamic analysis of thermophotovoltaic efficiency and power density tradeoffs. J Appl Phys 89:3319–3327. Doi:10.1063/1.1344580

Battaglia C, De Nicolas SM, De Wolf S et al (2014) Silicon heterojunction solar cell with passivated hole selective MoOx contact. Appl Phys Lett 104:2012–2017. Doi:10.1063/1.4868880

Beard MC (2011) Multiple exciton generation in semiconductor quantum dots. J Phys Chem Lett 2:1282–1288. Doi:10.1021/jz200166y

Boriskina SV, Green MA, Catchpole K et al (2016) Roadmap on optical energy conversion. J Opt 18:73004. Doi:10.1088/2040-8978/18/7/073004

Brandt RE, Mangan NM, Li JV et al (2016) Temperature- and intensity-dependent photovoltaic measurements to identify dominant recombination pathways. In: Proceedings of the 43rd IEEE photovoltaic specialist conference

Brown AS, Green MA (2002) Impurity photovoltaic effect: fundamental energy conversion efficiency limits. J Appl Phys 92:1329–1336. Doi:10.1063/1.1492016

Cuevas A (2014) The recombination parameter J_0. Energy Procedia 0:53–62. Doi:10.1016/j.egypro.2014.08.073

D'Innocenzo V, Grancini G, Alcocer MJP et al (2014) Excitons versus free charges in organo-lead tri-halide perovskites. Nat Commun 5:1–6. Doi:10.1038/ncomms4586

Deceglie MG, Silverman TJ, Marion B, Kurtz SR (2014) Metastable changes to the temperature coefficients of thin-film photovoltaic modules. In: 40th IEEE photovoltaic specialist conference. IEEE, Honolulu, HI, pp 337–340

Dey P, Paul J, Bylsma J et al (2013) Origin of the temperature dependence of the band gap of PbS and PbSe quantum dots. Solid State Commun 165:49–54. Doi:10.1016/j.ssc.2013.04.022

Dupré O (2015) Physics of the thermal behavior of photovoltaic devices. PhD thesis. INSA Lyon, France

Dupré O, Vaillon R, Green MA (2015a) Experimental assessment of temperature coefficient theories for silicon solar cells. IEEE J Photovolt 1–5. Doi:10.1109/JPHOTOV.2015.2489864

Dupré O, Vaillon R, Green MA (2015b) Physics of the temperature coefficients of solar cells. Sol Energy Mater Sol Cells 140:92–100. Doi:10.1016/j.solmat.2015.03.025
Emery K (2008) Photovoltaic test performance: laboratory test procedures measure photovoltaic cells and modules according to international standards. Photonics Spectra 42:76–80
Emery K, Burdick J, Caiyem Y et al (1996) Temperature dependence of photovoltaic cells, modules and systems. In: 25th IEEE photovoltaic specialists conference. IEEE, pp 1275–1278
Even J, Pedesseau L, Dupertuis MA et al (2012) Electronic model for self-assembled hybrid organic/perovskite semiconductors: reverse band edge electronic states ordering and spin-orbit coupling. Phys Rev B-Condens Matter Mater Phys 86:3–6. Doi:10.1103/PhysRevB.86.205301
Fan J (1986) Theoretical temperature dependence of solar cell parameters. Sol cells 17:309–315
Fraunhofer (2016) Photovoltaics report
Friedman DJ (1996) Modelling of tandem cell temperature coefficients. In: 25th IEEE photovoltaic specialists conference. IEEE, pp 89–92
Goni AR, Cantarero A, Syassen K, Cardona M (1990) Effect of pressure on the low-temperature exciton absorption in GaAs. Phys Rev B 41:10111–10119. Doi:10.1103/PhysRevB.41.10111
Green MA (1981) Solar cell fill factors: general graph and empirical expressions. Solid State Electron 2–3
Green MA (1982) Solar cells: operating principles, technology, and system applications. Prentice-Hall, Englewood Cliffs
Green MA (1990) Intrinsic concentration, effective densities of states, and effective mass in silicon. J Appl Phys 67:2944–2954. Doi:10.1063/1.345414
Green MA (2001) Third generation photovoltaics: ultra-high conversion efficiency at low cost. Prog Photovoltaics Res Appl 9:123–135. Doi:10.1002/pip.360
Green MA (2003) General temperature dependence of solar cell performance and implications for device modelling. Prog Photovoltaics Res Appl 11:333–340. Doi:10.1002/pip.496
Green MA (2006) Third generation photovoltaics. Springer, Berlin Heidelberg
Green MA (2012) Radiative efficiency of state of the art photovoltaic cells. Prog Photovolt Res Appl 20:472–476. Doi:10.1002/pip
Green MA, Emery K, Blakers AW (1982) Silicon solar cells with reduced temperature sensitivity. Electron Lett 18:97–98. Doi:10.1049/el:19820066
Green MA, Blakers AW, Osterwald CR (1985) Characterization of high-efficiency silicon solar cells. J Appl Phys 58:4402. Doi:10.1063/1.336286
Green MA, Ho-Baillie A, Snaith HJ (2014) The emergence of perovskite solar cells. Nat Photonics 8:506–514. Doi:10.1038/nphoton.2014.134
Green MA, Keevers MJ, Thomas I et al (2015) 40% efficient sunlight to electricity conversion. Prog Photovoltaics Res Appl 23:685–691. Doi:10.1002/pip.2612
Green MA, Emery K, Hishikawa Y, Warta W, Dunlop ED (2016) Solar cell efficiency tables (Version 48). Prog Photovoltaics Res Appl 24:905–913. Doi:10.1002/pip.2788
Grover S, Li JV (2015) Theory and analysis of temperature coefficient of open-circuit voltage (dV_{oc}/dT) in heterojunction solar cells. In: 42nd IEEE photovoltaic specialists conference, New Orleans
Grover S, Li JV, Young DL et al (2013) Reformulation of solar cell physics to facilitate experimental separation of recombination pathways. Appl Phys Lett. Doi:10.1063/1.4819728
Helmers H, Schachtner M, Bett AW (2013) Influence of temperature and irradiance on triple-junction solar subcells. Sol Energy Mater Sol Cells 116:144–152. Doi:10.1016/j.solmat.2013.03.039
Henry CH (1980) Limiting efficiencies of ideal single and multiple energy gap terrestrial solar cells. J Appl Phys 51:4494–4500. Doi:10.1063/1.328272
Hirst LC, Ekins-Daukes NJ (2011) Fundamental losses in solar cells. Prog Photovolt Res Appl 19:286–293. Doi:10.1002/pip.1024
Huldt L, Nilsson NG, Svantesson KG (1979) The temperature dependence of band-to-band Auger recombination in silicon. Appl Phys Lett 35:776. Doi:10.1063/1.90974
IEC (2008) Photovoltaic devices—part 3: measurement principles for terrestrial photovoltaic (PV) solar devices with reference spectral irradiance data, 2nd edn. In: Int. Stand., IEC 60904-3

Ishihara T (1994) Optical properties of PbI-based perovskite structures. J Lumin 60–61:269–274. Doi:10.1016/0022-2313(94)90145-7

Jiang Y, Soufiani AM, Gentle A et al (2016) Temperature dependent optical properties of $CH_3NH_3PbI_3$ perovskite by spectroscopic ellipsometry. Appl Phys Lett 108:61905. Doi:10.1063/1.4941710

Katz EA, Faiman D, Tuladhar SM et al (2001) Temperature dependence for the photovoltaic device parameters of polymer-fullerene solar cells under operating conditions. J Appl Phys 90:5343–5350. Doi:10.1063/1.1412270

Klaassen D (1992a) A unified mobility model for device simulation—I. Model equations and concentration dependence. Solid State Electron 35:953–959

Klaassen D (1992b) A unified mobility model for device simulation—II. Temperature dependence of carrier mobility and lifetime. Solid State Electron 35:961–967

Kosten EDE, Atwater JHJ, Parsons J et al (2013) Highly efficient GaAs solar cells by limiting light emission angle. Light Sci Appl 2:1–6. Doi:10.1038/lsa.2013.1

Kosten ED, Newman BK, Lloyd JV et al (2015) Limiting light escape angle in silicon photovoltaics: ideal and realistic cells. IEEE J Photovolt 5:61–69. Doi:10.1109/JPHOTOV.2014.2360566

Landis G (1994) Review of solar cell temperature coefficients for space. In: Proceedings of the 13th space photovoltaic research and technology conference, pp 385–399

Landsberg PT, Badescu V (2000) Carnot factor in solar cell efficiencies. J Phys D Appl Phys 33:3004–3008. Doi:10.1088/0022-3727/33/22/320

Li JV, Grover S, Contreras MA et al (2014a) A recombination analysis of Cu(In,Ga)Se2 solar cells with low and high Ga compositions. Sol Energy Mater Sol Cells 124:143–149. Doi:10.1016/j.solmat.2014.01.047

Li JV, Grover S, Repins IL et al (2014b) Electrical characterization of interface recombination and its dependence on band offset, potential barrier height, and inversion in certain heterojunction solar cells. In: 40th photovoltaic specialists conference. IEEE, pp 686–690. Doi:http://dx.doi.org/10.1109/PVSC.2014.6925013

Liou KN (2002) An introduction to atmospheric radiation. Academic Press, USA

Luque A, Martí A (1997) Increasing the efficiency of ideal solar cells by photon induced transitions at intermediate levels. Phys Rev Lett 78:5014–5017. Doi:10.1103/PhysRevLett.78.5014

Luque A, Martí A, Stanley C (2012) Understanding intermediate-band solar cells. Nat Photonics 6:146–152. Doi:10.1038/nphoton.2012.1

Markvart T (2008) Solar cell as a heat engine: energy-entropy analysis of photovoltaic conversion. Phys Status Solidi 205:2752–2756. Doi:10.1002/pssa.200880460

Martí A, Araújo GL (1996) Limiting efficiencies for photovoltaic energy conversion in multigap systems. Sol Energy Mater Sol Cells 43:203–222. Doi:10.1016/0927-0248(96)00015-3

Menard E, Meitl M, Burroughs S (2012) Indirect temperature measurement of CPV solar cells using wavelength shift of the sub-cells luminescence emission peaks. In: 27th European photovoltaic solar energy conference and exhibition, pp 189–193

Nell MME, Barnett AAM (1987) The spectral p-n junction model for tandem solar-cell design. IEEE Trans Electron Dev 34:257–266. Doi:10.1109/T-ED.1987.22916

Nozik AJ (2008) Multiple exciton generation in semiconductor quantum dots. Chem Phys Lett 457:3–11. Doi:10.1016/j.cplett.2008.03.094

Olkhovets A, Hsu RC, Lipovskii A, Wise F (1998) Size-dependent temperature variation of the energy gap in lead-salt quantum dots. Phys Rev Lett 81:3539–3542. Doi:10.1103/PhysRevLett.81.3539

Pässler R (1999) Parameter sets due to fittings of the temperature dependencies of fundamental bandgaps in semiconductors. Phys Status Solidi 216:975–1007. Doi:10.1002/(SICI)1521-3951(199912)216:2<975:AID-PSSB975>3.0.CO;2-N

Philipps SP, Hoheisel R, Gandy T et al (2011) An experimental and theoretical study on the temperature dependence of GaAs solar cells. In: 37th IEEE photovoltaic specialists conference, pp 001610–001614. Doi:10.1109/PVSC.2011.6186264

Ponce-Alcántara S, Connolly JP, Sánchez G et al (2014) A statistical analysis of the temperature coefficients of industrial silicon solar cells. Energy Procedia 55:578–588. Doi:10.1016/j.egypro.2014.08.029

Press WH (1976) Theoretical maximum for energy from direct and diffuse sunlight. Nature 264:734–735

Richter A, Hermle M, Glunz SW (2013) Reassessment of the limiting efficiency for crystalline silicon solar cells. IEEE J Photovoltaics 3:1184–1191. Doi:10.1109/JPHOTOV.2013.2270351

Riedel I, Parisi J, Dyakonov V et al (2004) Effect of temperature and illumination on the electrical characteristics of polymer-fullerene bulk-heterojunction solar cells. Adv Funct Mater 14:38–44. Doi:10.1002/adfm.200304399

Riesen Y, Stuckelberger M, Haug F-J et al (2016) Temperature dependence of hydrogenated amorphous silicon solar cell performances. J Appl Phys 119:44505. Doi:10.1063/1.4940392

Ross RT (1967) Some thermodynamics of photochemical systems. J Chem Phys 46:4590. Doi:10.1063/1.1840606

Ross RT, Nozik AJ (1982) Efficiency of hot-carrier solar energy converters. J Appl Phys 53:3813–3818. Doi:10.1063/1.331124

Ruppel W, Würfel P (1980) Upper limit for the conversion of solar energy. IEEE Trans Electron Devices 27:877–882. Doi:10.1109/T-ED.1980.19950

Schenk A (1992) A model for the field and temperature dependence of Shockley-Read-Hall lifetimes in silicon. Solid State Electron 35:1585–1596

Seif JP, Descoeudres A, Filipic M et al (2014) Amorphous silicon oxide window layers for high-efficiency silicon heterojunction solar cells. J Appl Phys. Doi:10.1063/1.4861404

Seif JP, Krishnamani G, Ballif C, De Wolf S (2015) Amorphous/ crystalline silicon interface passivation: ambient-temperature dependence and implications for solar cell performance. IEEE J Photovolt 5:718–724

Seif JP, Menda D, Descoeudres A et al (2016) Asymmetric band offsets in silicon heterojunction solar cells: impact on device performance. J Appl Phys 120:54501. Doi:10.1063/1.4959988

Shockley W (1948) The theory of p-n junctions in semiconductors and p-n junction transistors. Bell Syst Tech J 435–489. Doi:10.1002/j.1538-7305.1949.tb03645.x

Shockley W, Queisser HJ (1961) Detailed balance limit of efficiency of p-n junction solar cells. J Appl Phys 32:510–519. Doi:10.1063/1.1736034

Siefer G, Bett AW (2012) Analysis of temperature coefficients for III-V multi-junction concentrator cells. Prog Photovoltaics Res Appl 22:515–524. Doi:10.1002/pip

Siefer G, Abbott P, Baur C et al (2005) Determination of the temperature coefficients of various III–V solar cells. In: 20th European photovoltaic solar energy conference. Barcelona, Spain, pp 495–498

Singh P, Ravindra NM (2012) Temperature dependence of solar cell performance—an analysis. Sol Energy Mater Sol Cells 101:36–45. Doi:10.1016/j.solmat.2012.02.019

Singh P, Singh S, Lal M, Husain M (2008) Temperature dependence of I-V characteristics and performance parameters of silicon solar cell. Sol Energy Mater Sol Cells 92:1611–1616. Doi:10.1016/j.solmat.2008.07.010

Søndenå R, Berthod C, Odden JO et al (2015) Temperature dependent quantum efficiencies in multicrystalline silicon solar cells. Energy Procedia 77:639–645. Doi:10.1016/j.egypro.2015.07.093

Strevel N, Trippel L, Gloeckler M, Solar F (2012) First solar: greater energy yields in high-temperature conditions performance characterization and superior energy yield of first solar PV power plants in high-temperature conditions. Photovolt Int 1–6

Sze S, Ng K (1981) Physics of semiconductor devices. Wiley, New York

Taguchi M, Maruyama E, Tanaka M (2008) Temperature dependence of amorphous/crystalline silicon heterojunction solar cells. Jpn J Appl Phys 47:814–818. Doi:10.1143/JJAP.47.814

Tanay F, Dubois S, Enjalbert N, Veirman J (2011) Low temperature-coefficient for solar cells processed from solar-grade silicon purified by metallurgical route, pp 966–972. Doi:10.1002/pip

Tiedje T, Yablonovitch E, Cody GD, Brooks BG (1984) Limiting efficiency of silicon solar cells. IEEE Trans Electron Devices 31:711–716. Doi:10.1109/T-ED.1984.21594

Trupke T, Green MA, Würfel P (2002) Improving solar cell efficiencies by up-conversion of sub-band-gap light. J Appl Phys 92:4117–4122. Doi:10.1063/1.1505677

Trupke T, Green MA, Würfel P et al (2003) Temperature dependence of the radiative recombination coefficient of intrinsic crystalline silicon. J Appl Phys 94:4930–4937. Doi:10.1063/1.1610231

Varshni YP (1967) Temperature dependence of the energy gap in semiconductors. Physica 34:149–154. Doi:10.1016/0031-8914(67)90062-6

Virtuani A, Pavanello D, Friesen G (2010) Overview of temperature coefficients of different thin film photovoltaic technologies. In: 25th European photovoltaic solar energy conference

Vurgaftman I, Meyer JR, Ram-Mohan LR (2001) Band parameters for III-V compound semiconductors and their alloys. J Appl Phys 89:5815–5875. Doi:10.1063/1.1368156

Wu K, Bera A, Ma C et al (2014) Temperature-dependent excitonic photoluminescence of hybrid organometal halide perovskite films. Phys Chem Chem Phys 16:22476–22481. Doi:10.1039/C4CP03573A

Würfel P (1982) The chemical potential of radiation. J Phys C: Solid State Phys 15:3967–3985. Doi:10.1088/0022-3719/15/18/012

Würfel P (2009) Physics of solar cells: from basic principles to advanced concepts. Wiley, New York

Xiao C, Yu X, Yang D, Que D (2014) Impact of solar irradiance intensity and temperature on the performance of compensated crystalline silicon solar cells. Sol Energy Mater Sol Cells 128:427–434. Doi:10.1016/j.solmat.2014.06.018

Xu P, Chen S, Xiang H-J et al (2014) Influence of defects and synthesis conditions on the photovoltaic performance of perovskite semiconductor CsSnI3. Chem Mater 26:6068–6072. Doi:10.1021/cm503122j

Yoon S, Garboushian V (1994) Reduced temperature dependence of high-concentration photovoltaic solar cell open-circuit voltage (Voc) at high concentration levels. In: 1st world conference on photovoltaic energy conversion—WCPEC (A Joint Conference of PVSC, PVSEC and PSEC). IEEE, pp 1500–1504

Yu C, Chen Z, Wang J et al (2011) Temperature dependence of the band gap of perovskite semiconductor compound CsSnI3. J Appl Phys 110:63526. Doi:10.1063/1.3638699

Zhao J, Wang A, Robinson SJ, Green MA (1994) Reduced temperature coefficients for recent high performance silicon solar cells. Prog Photovoltaics Res Appl 2:221–225. Doi:10.1002/pip.4670020305

http://www.springer.com/978-3-319-49456-2

Thermal Behavior of Photovoltaic Devices
Physics and Engineering
Dupré, O.; VAILLON, R.; Green, M.A.
2017, XIV, 130 p. 58 illus., 55 illus. in color., Hardcover
ISBN: 978-3-319-49456-2